A nanoporous capacitive electrochemical ratchet for continuous ion separations

Rylan Kautz[1], Alon Herman[2], Ethan J. Heffernan[1], Camila Muñetón[3,4], David Larson[5,6], Joel W. Ager III[5,6,7,8], Francesca M. Toma[5,6,9], Shane Ardo[1,3,10]* and Gideon Segev[2,5,6]**

[1]Department of Materials Science & Engineering, University of California Irvine, Irvine, CA 92697, USA
[2]School of Electrical Engineering, Tel Aviv University, Tel Aviv 6997801, Israel
[3]Department of Chemistry, University of California Irvine, Irvine, CA 92697, USA
[4]Department of Chemistry, University of Massachusetts Boston, Boston, MA 02125 USA
[5]Chemical Sciences Division, Lawrence Berkeley National Lab, Berkeley, CA 94720, USA
[6]Joint Center for Artificial Photosynthesis, Lawrence Berkeley National Lab, Berkeley, CA 94720, USA
[7]Materials Sciences Division, Lawrence Berkeley National Lab, Berkeley, CA 94720, USA
[8]Department of Materials Science and Engineering, University of California Berkeley, Berkeley, CA 94720, USA
[9]Institute of Functional Materials for Sustainability, Helmholtz Zentrum Hereon, Teltow, 14513, DE
[10]Department of Chemical & Biomolecular Engineering, University of California Irvine, Irvine, CA 92697, USA

*Email: ardo@uci.edu
**Email: gideons1@tauex.tau.ac.il

Abstract

Directed ion transport in liquid electrolyte solutions underlies many phenomena in Nature and industry. While Nature has devised structures that drive continuous ion flow without Faradaic redox reactions, artificial analogs do not exist. Here we report the first demonstration of an ion pump that drives aqueous ions against a force using a capacitive ratchet mechanism that does not require redox reactions. Modulation of an electric potential between gold thin films on either face of a nanoporous alumina wafer immersed in solution resulted in persistent voltages and ionic currents indicative of directional ion pumping. This occurs due to the non-linear capacitive nature of electric double layers, whose repeated charging and discharging sustains a continuous ion flux. The generated ionic power was used in conjunction with an additional shunt pathway to demonstrate electrolyte demixing. These ratchet-based ion pumps can potentially enable continuous desalination and selective ion separation using a modular, electrically powered device with no moving parts.

Main

Ratchets are non-equilibrium devices that utilize temporally modulated input signals and spatial asymmetries to drive a steady state particle flux.[1–3] Ratchets have been studied theoretically and experimentally[2–7] for electronic signal rectification,[1–10] to drive net transport of uncharged species through induced-charge electrokinetics,[11] for microparticle and nanoparticle sorting,[12–18] and to drive

net ionic current or water pumping by alternating redox reactions.[19–21] A recent theoretical study has shown that ratchet based ion pumps (RBIPs) can sort ions with unprecedented selectivity.[22]

An electric double layer forms at the interface between an electrode and a liquid electrolyte and consists of a compact layer of adsorbed solvent molecules and ions, and a diffuse layer of mobile ions. This results in a capacitance that varies with the magnitude of the electrode potential and in response to temporal changes in it.[23–25] These variations in capacitance affect the double layer charging and discharging time constants. Here we utilize this phenomenon to pump ions across a membrane. RBIP membranes are made of nanoporous anodized aluminum oxide (AAO) wafers with thin gold layers, serving as electrodes covering the two wafer surfaces without blocking the pores, thus forming nanoporous capacitor-like structures (Figure 1a-e, S1). Details on the RBIP fabrication process can be found in the methods section. Due to the rough and poly-crystalline nature of the gold films covering the AAO wafer (Figure 1b,c), the RBIP surface is inhomogeneous. Moreover, the energetics of Cl^- adsorption processes are facet dependent.[26] Collectively, these result in potential-dependent adsorption and charging phenomena on the RBIP surfaces leading to a dispersion of time constants and thus a non-linear capacitance.[24–27] Since no two poly-crystalline surfaces are identical, small differences in the RBIP surface properties result in an unintentional asymmetry, which is essential for ratchet-driven transport.

When an input signal, V_{in}, is applied between the two metal layers, the double layer at one surface is charged while the other is discharged with time constants that are determined by the properties of the input signal, the metal surface, and the aqueous electrolyte. The electrostatic potential difference between the bulk solution and the adjacent metal surface at each side of the RBIP (V_L and V_R in Figure 1a) fluctuates according to these time constants, and the electric potential difference between the bulk of the two electrolyte compartments is:

$$V_{out}(t) = V_L(t) + V_{in}(t) - V_R(t) \quad (1)$$

The RBIP performance was evaluated by placing an RBIP between two compartments of aqueous chloride-containing electrolyte and measuring the voltage between two Ag/AgCl wires, which are immersed in the solution on each side of the RBIP (V_{out}). Because of the extremely high reaction rate for reversible oxidation of Cl^- at Ag to form insoluble AgCl, the voltage difference between the two Ag/AgCl wires is dominated by the electrochemical potential difference of Cl^- at the wire surfaces. The measured resting voltage between the two Ag/AgCl wires, V_{rest}, when both compartments are filled with the same electrolyte (1 – 10 mM Cl^- containing solution) is lower than 10 mV in magnitude and is typically about 3 mV. Application of a DC bias across the RBIP gold contacts (V_{in} of +300 mV or –300 mV) resulted in the expected prompt observation of $V_{out} \approx V_{in}$ that decayed to $V_{out} \approx V_{rest}$ over ~1 sec due to capacitive charging. Hence, under these conditions there is no steady state net driving force for ion transport through the RBIP.

To demonstrate the difference in charging and discharging time constants and their contribution to the ratchet output, the voltage signals $V_L(t)$ and $V_R(t)$ were measured while the RBIP was operating. The input signal was a rectangular wave in the form:

$$V_{in}(t) = \begin{matrix} V_a & 0 < t \le d_c T \\ -V_a & d_c T < t \le T \end{matrix} \quad (2)$$

where T is the temporal period and d_c ($\in [0,1]$) is the duty cycle. The charging and discharging time constants of every surface at every part of the period were found by fitting the averaged measured signals to a single exponential charging/discharging function:

$$V(t) = \begin{cases} V_{f,1} + (V_{i,1} - V_{f,1})\exp\left(-\frac{t}{\tau_1}\right) & 0 < t \leq d_c T \\ V_{f,2} + (V_{i,2} - V_{f,2})\exp\left(-\frac{t - d_c T}{\tau_2}\right) & d_c T < t \leq T \end{cases} \quad (3)$$

where V_i is the initial voltage, and τ is the charging/discharging time constant. V_f is the voltage at which the signal would saturate if the capacitances were linear. A subscript 1 notes the first part of the temporal period ($0 < t \leq d_c T$) and a subscript 2 the second part of the period ($d_c T < t \leq T$).

Because the RBIP is electrically floating (i.e., no part of the system is grounded), charging of one contact is accompanied by discharging of the other (Figure 1f-g). Thus, the time constants for charging the right and left surfaces are $\tau_{R,1}$ and $\tau_{L,2}$ respectively, and the time constants for discharging the right and left surfaces are $\tau_{R,2}$ and $\tau_{L,1}$ respectively. Figure 1h shows the extracted time constants for charging and discharging the surfaces as a function of the duty cycle. The other fitted parameters are shown in Figure S2. In linear systems the time constants are invariant. However, due to the non-linearity of the double layer capacitances, all time constants vary with the duty cycle. Particularly, there is a significant difference between the charging (and discharging) time constants of the two surfaces: $\tau_{L,1} \neq \tau_{R,2}$ and $\tau_{L,2} \neq \tau_{R,1}$. At a duty cycle of 0.5 the time constants are: $\tau_{L,1} = 6.59$ ms, $\tau_{R,2} = 8.21$ ms, and $\tau_{L,2} = 8.5$ ms, $\tau_{R,1} = 7.23$ ms. This asymmetry implies that a voltage rise due to the charging of a surface at the first part of the period is not fully negated by the charging of the opposite surface during the second part of the period. As a result, a non-zero time-averaged output voltage can be obtained even for time symmetric input signals. For duty cycles above 0.4 the time constants for charging one surface and discharging the other are similar yet vary significantly between the first part and the second part of the period: $\tau_{L,1} \approx \tau_{R,1} \neq \tau_{L,2} \approx \tau_{R,2}$. A similar analysis for signals with different frequencies and $d_c = 0.5$ shows that the time constants decrease significantly with the signal frequency (Figure S4-5). Thus, the charging and discharging dynamics are mostly determined by the duration for charging and discharging. As a result, the difference in charging and discharging time constants is smallest for $d_c = 0.5$, and for this duty cycle the asymmetry is determined by the non-linear nature of the capacitance with the potential and the difference in the microstructure of the two surfaces.

The net ratchet induced voltage, $\Delta\bar{V}_{out}$, was obtained by finding the mean value of V_{out} while the ratchet is ON and reducing from it the mean value of V_{out} while the ratchet was OFF (see the methods section and Figure S3 for more details). Figure 1i shows $\Delta\bar{V}_{out}$ as a function of the input signal duty cycle. Demonstrating the signature output of a flashing ratchet,[1,4] the RBIP output is very low when a constant bias is applied (duty cycle of 0 or 1). However, once the input signal alternates, a net voltage builds up between the two compartments providing a driving force for ion transport. Moreover, $\Delta\bar{V}_{out}$ reaches 29.1 mV for a moderate duty cycle of 0.375 where the time averaged input is -75 mV, and 23 mV for a duty cycle of 0.5 where the time averaged input voltage is 0 V. Since $\Delta\bar{V}_{out}$ is maximal when the time-averaged input voltage is near 0 V, and it is negligible for extreme duty cycles when the magnitude of the time-averaged input voltage is maximal, it can be concluded that the contribution of mechanisms such as conduction, ion electrophoresis and electro-osmosis is minimal. This was further verified by showing that mass transport of water through the membrane is negligible (Figures S12-13).

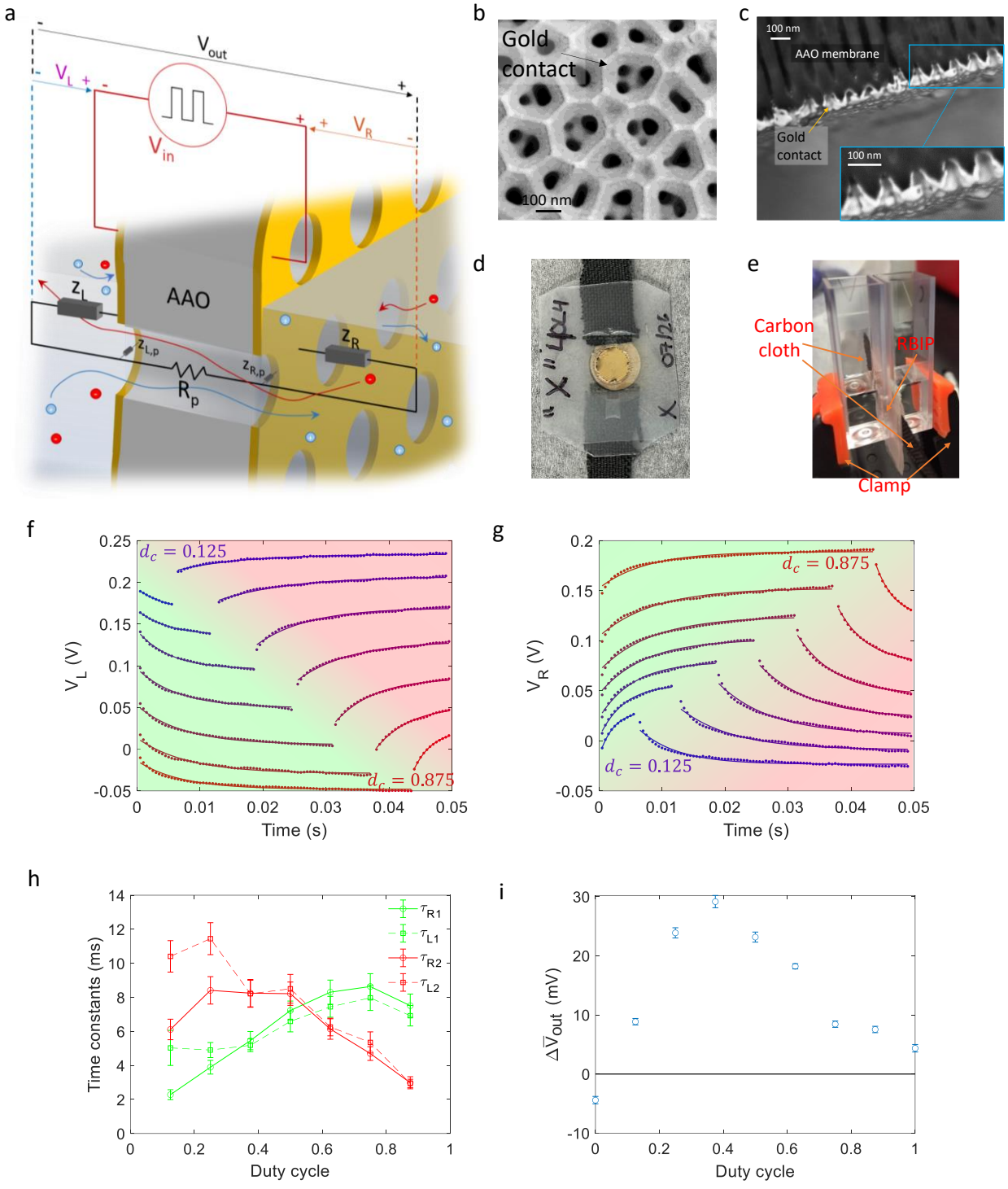

Figure 1: The RBIP|(a) A schematic illustration of the RBIP structure and double layers impedances. (b-c) Plan and cross section view SEM images of fabricated RBIPs respectively. (d) A photograph of a sample before its assembly. (e) A photograph of the RBIP performance characterization setup. Figure S1 shows an illustration of the mounting process of an RBIP sample in the electrochemical cell. (f-g) Experimentally measured signals $V_L(t)$ and $V_R(t)$, respectively, for rectangular-wave inputs with various duty cycles, d_c, over one time period, T=50 ms. The green areas are for the first portion of the period $0 < t \leq d_c T$ and the red areas are for the second portion of the period $d_c T < t \leq T$. The dots are the measurements, and the solid lines mark the

best exponential fit to the data. The color coding marks the duty cycle and is the same in both (f) and (g). The electrolyte is 1 mM KCl aqueous solution, and the input signal is alternating between 300 mV and -300 mV. (h) Time constants extracted from the fitted curves in (f) and (g). Subscripts 1 and 2 denote that the time constants were extracted for the first ($0 < t \leq d_c T$) and second ($d_c T < t \leq T$) parts of the input signal, respectively. The error bars indicate the fitting 95% confidence interval. (i) The time averaged output voltage $\Delta\bar{V}_{out}$ as a function of the input signal duty cycle.

Next, we measured the ratchet performance for input signals with various frequencies and duty cycles. Figure 2a shows the averaged temporal response, V_{out}, at a duty cycle of 0.5 and several frequencies. The data for other duty cycles is shown in Figure S6. Figure 2b shows the time constants extracted from V_{out} as a function of the duty cycle and frequency. Similar to the trends observed in Figure 1h and Figure S5, the time constants vary with the input signal duty cycle and decrease significantly its frequency. Figure 2c shows $\Delta\bar{V}_{out}$ as a function of the duty cycle and frequency. As in Figure 1i, here also $\Delta\bar{V}_{out}$ is practically zero for extreme duty cycles and low frequencies when the device is effectively at its steady state for significant parts of the temporal period. $\Delta\bar{V}_{out}$ increases with the input signal frequency reaching about -17 mV at a frequency of 250 Hz and a duty cycle of 0.6. Although the RBIP output increases with frequency within this range, it decreases for higher frequencies (Figure S9 and Figure S14).

$\Delta\bar{V}_{out}$ values for an aqueous 1 mM electrolyte were observed to be larger than $\Delta\bar{V}_{out}$ values for an aqueous 10 mM electrolyte (Figure S9). Since the resistance for charge transport through the pore, R_p, effectively shunts $\bar{V}_{out}$ (Figure 1a), solutions with high ionic strength and membranes with a large pore diameter will tend to produce a lower RBIP output. The ionic strength of the solution also affects the double layer capacitances and the charging and discharging time constants at the RBIP surfaces leading to higher optimal frequencies (Figure S9). We observed that the diminished performance with higher concentration solutions can be partially mitigated using AAO membranes with smaller pores, but at the expense of higher overall ionic resistance per pore (Figure S14). Ratcheting was also demonstrated with $\Delta\bar{V}_{out}$ measured between two leak-free reference electrodes. Since reference electrodes measure the electric potential, this allows decoupling between the electric and chemical potentials that are induced by the ratchet (Figure S11a,b). More details on the measurement of $\Delta\bar{V}_{out}$ and the output dependence on different input signals and solution parameters can be found in the supporting information.

The buildup of $\bar{V}_{out}$ results in the separation of cations and anions until columbic forces negate the ratchet action preventing further charge transport. Hence, to drive a sustained net ionic current, charge neutrality must be maintained. This can be achieved by electrically shorting the two Ag/AgCl wires, which provides a low resistance path for removing chlorides from one compartment and generating them in the other. In this case, the current between the Ag/AgCl wires, I_{out}, is a result of oxidation of one silver wire and an aqueous chloride to form silver chloride, and reduction of silver chloride on the other wire to form silver and an aqueous chloride. The generation of chlorides in one compartment and their removal in the other balances deviations from electroneutrality due to ion pumping driven by charging and discharging of the RBIP contacts. Figure 2d shows the net ratchet induced current density output $\Delta\bar{I}_{out}/A$ as a function of the input signal duty cycle and frequency. As the voltage output, the current output shows a flashing rachet-like behavior with zero net output current at duty cycles of 0 and 1. Once an alternating input signal is injected to the device, a significant output current flows reaching as much as 3.15 μA/cm^2 at a frequency of 250 Hz and a duty cycle of 0.6. Figures S7-8 show the average temporal response and the extracted time constants for all frequencies and duty cycles.

To demonstrate the RBIP ability to drive ions against a force, a current-voltage scan was taken between the two Ag/AgCl wires while the ratchet is OFF (V_{in} = 0 V) and when it was ON with a duty cycle of 50% and a frequency of 100 Hz (Figure 2e). When the ratchet is OFF, the curve shows an expected linear ohmic behavior. This is in contrast to membranes with conical nano-pores that were shown to have a rectifying transport behavior.[19,20] However, when the ratchet is ON, the curve shifts by approximately the same $\Delta\bar{V}_{out}$ that was measured under the same conditions, thus entering a quadrant in which ions are driven against an electrostatic force. It is interesting to analyze this result through the redox potentials of the Ag/AgCl wires. When the ratchet is OFF, the CV curve of the two Ag/AgCl wires follows a simple resistive form in which Cl^- is oxidized at the positively biased Ag/AgCl wire yielding an anodic current. However, once the ratchet is ON, the onset for this anodic reaction is shifted and Cl^- is oxidized even at voltages below 0 V. Complementary, the onset of the cathodic reaction is also shifted such that a negative overpotential of about 15 mV is required to drive a cathodic current.

Since the current voltage curve is linear, the energetic efficiency of the RBIP is approximately $\eta = 0.25V_{oc}I_{sc}/\bar{P}_{in}$ where V_{oc} and I_{sc} are the open circuit voltage and the short circuit current as shown in Figure 2c,d respectively and $\bar{P}_{in}$ is the time averaged input power. At a frequency of 250 Hz and a duty cycle of 50%, the input power is approximately 0.215 mW, and with the corresponding output from Figure 2c,d results in an efficiency of about $\eta = 1.96 \cdot 10^{-5}$. Notably, asymmetry was not introduced intentionally to the fabricated devices. Engineering devices for increased spatial asymmetry will result in increased asymmetrical charging and thus enhanced performance. This can be achieved by choosing different materials for the two metallic surfaces and by varying the deposition process of the two metallic layers. Using highly porous structures can also introduce geometric effects that can result in non-linear capacitances at higher frequencies.[27]

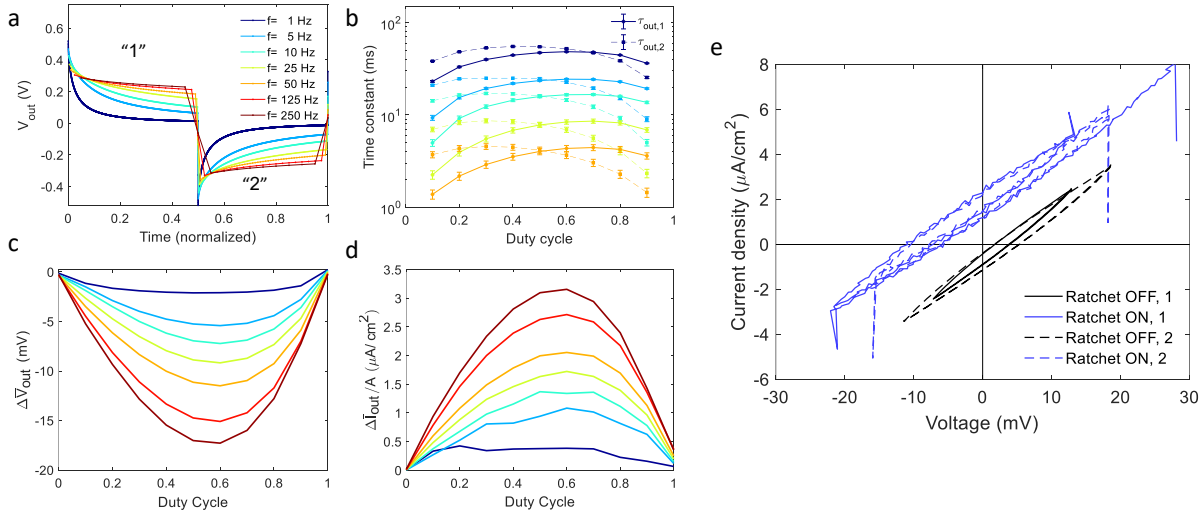

Figure 2: RBIP performance examination|(a) Vout as a function of time (normalized by the period, T) for several input signal frequencies and a duty cycle of 0.5. (b) The time constants of Vout for several input signal frequencies and duty cycles. (c) $\Delta\bar{V}_{out}$ as a function of the input signal duty cycle frequency. (d) The ratchet net output current density $\Delta\bar{I}_{out}/A$ as a function of the input signal duty cycle and frequency. The color coding for the input signal frequency is as in (a). (e) Current–Voltage curves ($\bar{I}_{out}/A$, $\bar{V}_{out}$) with Vin = 0 and with a square-wave input at a duty cycle of 0.5 and a frequency of 100 Hz. In all these measurements the electrolyte is 1 mM HCl aqueous solution, the RBIP pore diameter is 40 nm, the active area of the membrane is A = 0.32 cm2, and the input signal amplitude is Va = 0.3 V.

As discussed above, for a significant concentration gradient to develop, charge neutrality must be maintained within the two compartments. This can be achieved by driving the ratchet while two Ag/AgCl auxiliary electrodes are shunted across the RBIP to provide a low-impedance pathway for electronic current to flow and an ample capacity of solid AgCl. Figure 3a shows a schematic illustration of such a system. By removing Cl^- from the solution through oxidation at one auxiliary electrode and generating Cl^- on the other, the shorted auxiliary electrodes assure that charge neutrality is maintained regardless of differences in ratchet-induced chloride and cation currents. Thus, when cations are pumped by the RBIP into one compartment, chlorides are generated there to compensate for any additional positive charge, leading to an increase in electrolyte concentration. At the same time, since cations leave the other compartment and chlorides are removed through the auxiliary electrode, the electrolyte concentration in this compartment is reduced. As the cation concentration builds in one compartment and decreases in the other, the ability to net pump cations decreases due to back diffusion of cations. After a sufficiently long time, the force exerted by the ratchet will be equal to the force induced by the opposing concentration gradient and cations will no longer be transported through the RBIP. At this stage $\bar{I}_{aux}$ will be at a magnitude that supports the ratchet induced current and back diffusion without violating electroneutrality in either compartment.

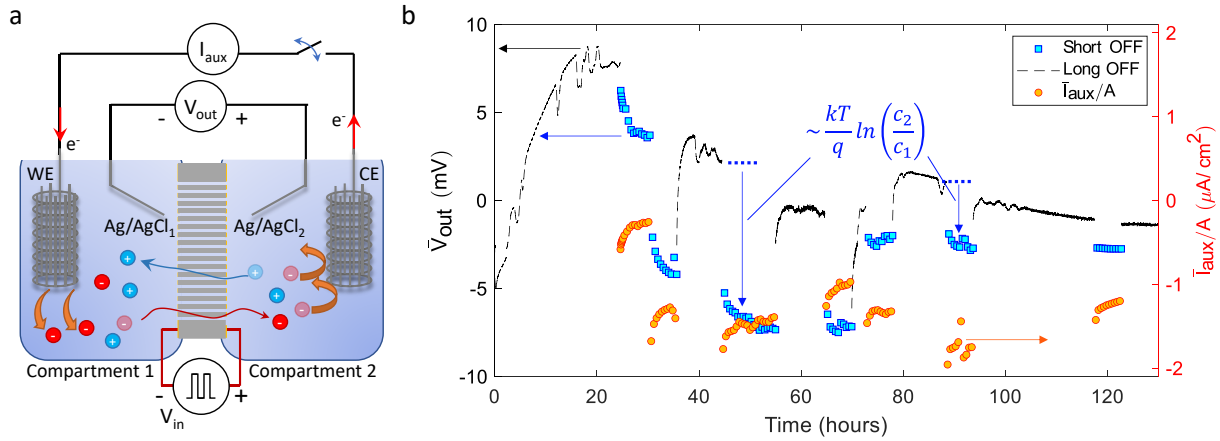

Figure 3: *Demixing demonstration| (a) Schematic illustration of an electrochemical cell used to demonstrate electrolyte demixing. (b) The Ag/AgCl wires time-averaged voltage, $\bar{V}_{out}$. Blue markers are measurements taken while the ratchet was OFF for short intervals between periods of ratchet operation, and the black dashed lines are measurements taken while the system is continuously at rest. The orange markers are the average current density measured between the Ag/AgCl auxiliary electrodes during every ratchet ON period. The input signal is a rectangular wave with a duty cycle of 0.5, frequency of 125 Hz and an amplitude, V_a, of 0.3 V. The solution is 1 mM HCl aqueous solution, the RBIP pore diameter is 40 nm, the active area of the membrane is A = 0.32 cm².*

RBIP-driven electrolyte demixing was demonstrated with a setup as illustrated in Figure 3a. Two Ag/AgCl wire meshes were used as auxiliary electrodes, and a set of Ag/AgCl wires was used to measure the chloride electrochemical potential difference between the two compartments. The RBIP sample had the same parameters as the one discussed in Figure 2 and the input signal was a square wave with duty cycle of 0.5, frequency of 125 Hz and an amplitude, V_a, of 0.3 V. Output characterization measurements for this sample are shown in Figure S15a-b. For the first 24 hours the system was at rest allowing it to equilibrate. Then, to demonstrate demixing, the RBIP was operated continuously with the auxiliary electrodes shunted, thus concentrating the solution in one compartment, and diluting the solution in

the other compartment as described above. Next, the ratchet was turned OFF (i.e., V_{in} = 0 V) for short intervals of 30 or 90 seconds and V_{out} was measured. The auxiliary electrodes current, I_{aux}, was not measured while the ratchet was OFF, thus the auxiliary electrodes were not shunted during these intervals (illustrated by the opening of the switch in Figure 3a). After several cycles of long operation and short ratchet OFF intervals, the ratchet was turned OFF for several hours and the system was allowed to equilibrate. This entire process was repeated multiple times as described in the methods section. Figure 3b shows the measured voltage for six periods of operation over the course of 5 days. Figure S16 shows in more detail the first three operation periods. The blue markers in Figure 3b mark the average voltage within each short OFF interval. The dashed black curves are the voltages measured during the long OFF durations. The orange markers are the time-averaged current density, $\bar{I}_{aux}/A$, measured while the ratchet is ON (normalized by the RBIP active area). The slow drift in voltage observed while the system is at rest (dashed black curves) is attributed to slow changes in the Ag/AgCl wires. When the cell was allowed to equilibrate with V_{in} = 0 V over the course of at least one day, it attained an exceptionally stable and low voltage near $0\ V$. However, following ratchet operation, a non-negligible and consistent offset of $\bar{V}_{out}$ is observed demonstrating electrolyte demixing. The short time interval in which the ratchet was OFF and V_{out} was measured is sufficient for discharging of the double layers, but too short to allow for any meaningful back diffusion of ions. Thus, the voltage offset is a result of the chemical potential difference of chlorides between the two compartments and the electrostatic potential difference induced by the permselectivity of the membrane.[28] Examples for this offset, which is approximately $kT/qln(c_2/c_1)$, are marked with the vertical arrows in Figure 3b (k, T, and q being the Boltzmann constant, the temperature, and the elementary charge, respectively, and c_1 and c_2 are respectively the Cl^- concentration in compartments 1 and 2). The cathodic current induced by the ratchet results in reduction of AgCl(s) to generate aqueous Cl^- in compartment 1 where the working electrode is located (WE in Figure 3a), and a decrease in the aqueous Cl^- concentration in compartment 2 where Cl^- is consumed by the counter electrode (CE in Figure 3a) via oxidation of Ag(s) to form AgCl(s). As a result, the developed chemical potential difference, $kT/qln(c_2/c_1)$, is negative as shown in Figure 3b. The correlation between the concentration ratio and the measured voltage was calibrated by measuring the resting voltage between the two compartments with various concentration ratios (Figure S17). The maximal voltage offset induced by the ratchet (relative to adjacent resting periods) was -7 mV. Using the calibration curve, this translates to a maximal concentration ratio of about 0.78 between the two compartments. Over the course of the week, the output of the ratchet was reduced due to sample degradation. Further discussion of device degradation and other failure modes can be found in the supporting information.

The ratchet performance can be simulated by assuming that the voltages V_L and V_R follow a charging and discharging behavior as in equation (3), and inserting them and the input signal into equation (1). The non-linear nature of the double layer impedances is approximated by assigning different time constants for the surfaces charging and discharging. Since these time constants are determined mostly by the duration of the charging and discharging period (Figure 1h, Figure S5a), it can be assumed that $\tau_{l,2} = \tau_{r,2}$ and $\tau_{l,1} = \tau_{r,1}$. $\Delta\bar{V}_{out}$ was calculated using this procedure for various input signals and time constants. More details on the computational model can be found in the supporting information. Figure 4a shows the normalized output, $\Delta\bar{V}_{out}/V_a$, as a function of the duty cycle for several input signal frequencies. The charging and discharging time constants are $\tau_{L,2} = \tau_{R,2} = 8$ ms, $\tau_{L,1} = \tau_{R,1} = 2$ ms which are close to those extracted from experiment (Figure 1h). The output curves show a ratchet behavior with outputs near zero for extreme duty cycles and low frequencies, in which the temporal

periods are significantly longer than the charging and discharging time constants. Like the experimental results, the output reaches largest magnitudes at moderate duty cycles and higher frequencies. Figure 4b shows similar curves for $\tau_{L,2} = \tau_{R,2} = 100$ ms and $\tau_{L,1} = \tau_{R,1} = 1$ ms. For such extreme time constants, the output is higher and the optimal duty cycle shifts toward 0. In both cases, the output saturates when increasing the frequency. Figure 4c shows the maximal normalized output (in terms of absolute values) as a function of $\tau_{R,1}$ and $\tau_{R,2}$, with $\tau_{L,1} = \tau_{R,1}$ and $\tau_{L,2} = \tau_{R,2}$, and Figure 4d shows corresponding duty cycles. The parameters used in Figure 4a,b are marked with a triangle and a diamond respectively. When the RBIP capacitance is linear, i.e. all the time constants are equal, the output is zero. However, the output increases with the difference in time constants reaching magnitudes that approach $2V_a$ at optimal duty cycles that shift toward 0 or 1. Hence, for the highest performance, the time constants for charging and discharging must be as far apart as possible. It should be noted that devices with a geometrical asymmetry but with a linear capacitance, i.e. $\tau_{R,1} = \tau_{R,2}$ and $\tau_{L,1} = \tau_{L,2}$, produce a zero output. Thus, optimizing electrodes for high frequency dispersion is essential for efficient RBIP operation.

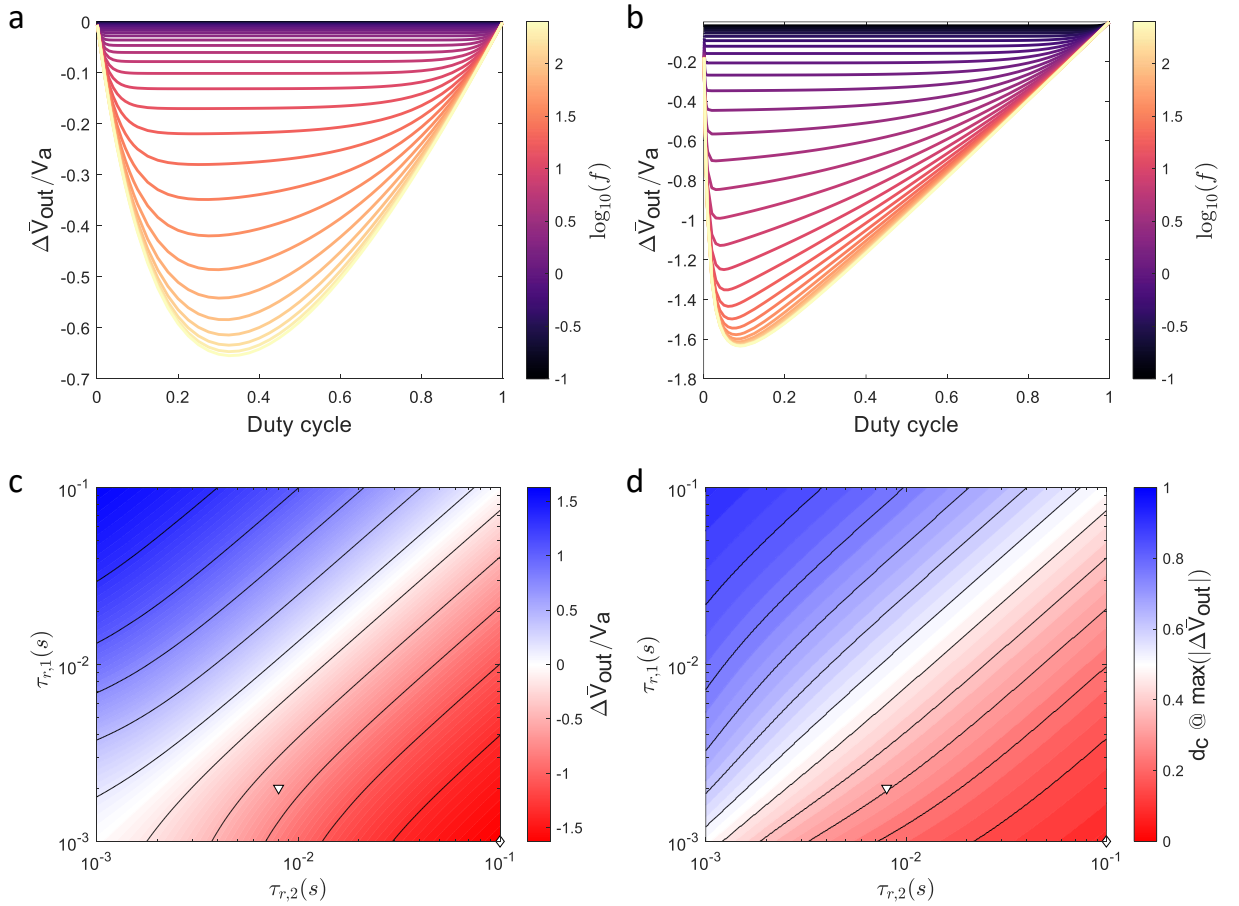

Figure 4: Device simulation *| (a) The ratchet normalized output, $\Delta\bar{V}_{out}/V_a$, as a function of the input signal duty cycle for several input signal frequencies and $\tau_{L,2} = \tau_{R,2} = 8$ ms, $\tau_{L,1} = \tau_{R,1} = 2$ ms. (b) $\Delta\bar{V}_{out}/V_a$ as a function of the input signal duty cycle for several input signal frequencies and $\tau_{L,2} = \tau_{R,2} = 100$ ms, $\tau_{L,1} = \tau_{R,1} = 1$ ms. (c) The RBIP normalized output, $\Delta\bar{V}_{out}/V_a$, as a function of $\tau_{R,1}$ and $\tau_{R,2}$. For each combination of time constants the duty cycle is optimized to obtain the highest output. The input signal frequency is 100 Hz. (d) The duty cycles for which the magnitude of $\bar{V}_{out}$ is maximal. The triangle and the diamond mark the parameters used in a and b respectively. In all the simulations $V_a = 0.3\ V$.*

The proposed model demonstrates that a non-linear capacitance, as observed in electric double layers, can result in a ratchet-like behavior. However, since the time constants in real devices vary significantly with the input signal properties, this model cannot predict the experimental performance of real devices and can only define optimal time constants for specific input signals. A detailed discussion of the model limitations can be found in the supporting information.

RBIPs can serve as building blocks in ion pumping systems operating with no redox reactions. For example, a dialysis system can be constructed from two RBIPs placed in parallel between two electrolyte compartments where each RBIP is designed to transport either anions or cations. Figure S25 shows a schematic illustration of such a system. Building on top of the suggested structures, more complex devices can be fabricated which can support an enhanced functionality. For example, layered structures can result in an ion pump driven with a flashing ratchet mechanism. The energetic efficiency of flashing ratchet-based dialysis was compared to reverse osmosis and was shown to be higher under a wide range of conditions.[29] In addition, we showed that RBIPs can theoretically drive ions of the same charge, but different diffusion coefficients, in opposite directions as well as to transport both cations and anions in the same direction.[22,30] Such devices can pave the way towards ion selective pumps and single membrane dialysis systems. Further increasing the number of metal layers connected to independent voltage sources may allow tailoring the potential distribution within the pores which can further increase the device functionality and efficiency.[7]

In conclusion, we have realized a first-of-its-kind ion pump driven by a capacitive ratchet mechanism. This type of ion pump can drive a net ion flux in steady state with no redox reactions at the RBIP contacts. Ion pumping against an opposing force was demonstrated as well as electrolyte demixing. The driving mechanism stems from the non-linear capacitance of electrode double layers, which leads to deviation in time constants between charging and discharging. The demonstrated ion pump can pave the way for the development of high efficiency desalination and selective ion separation systems, requiring neither moving parts nor redox reactions.

Methods

Sample preparation

RBIP samples were fabricated by depositing metal contacts on both surfaces of annealed anodized aluminum oxide (AAO) wafers (InRedox Materials Innovation) with pore diameters of 20 nm, 40 nm, or 60 nm. The wafers were air annealed for ~10 h at a temperature of 650 °C. Several RBIP structures and recipes were tested all showing qualitatively similar results. The samples discussed in Figure 2-3 were made of AAO wafers with a pore diameter of 40 nm and their contacts were deposited with thermal evaporation of a chrome adhesion layer and then gold. The thickness of both layers was 40 nm (planar equivalent). The sample discussed in Figure 1 had a pore diameter of 60 nm and the metal contacts were deposited with magnetron sputtering of gold (50 nm planar equivalent) followed by an 8 nm thick TiO_2 coating deposited by ALD. The ALD recipe is as described by Vega et al.[31] where the exposure time to the precursors was set to 1 s and the purging time was set to 5 s. The edges of the sample were masked during the ALD process to allow contacting the sample. The metal contacts in the samples described in Figures S9, S14 were deposited with electron beam evaporation of a 10 nm thick titanium adhesion layer and then 40 nm of gold. The RBIP ion pumping properties were tested in an electrochemical cell in which the RBIP served as a membrane separating two aqueous electrolyte

compartments, each containing an Ag/AgCl wire that was used to probe the voltage or current between the two compartments. In the experiments shown in Figures 2-3, parafilm was used to secure the wafers and prevent leakage. The hole diameter between each well is 0.32 cm^2 – this area is used for determining current density. Carbon black cloth was used to contact the RBIPs electrodes. In the experiments presented in Figures 2-3 each compartment in the electrochemical cell was filled with 1 mL of electrolyte.

RBIP performance characterization

To ensure that all the observed performance is a result of a ratcheting mechanism, as opposed to artifacts induced by unwanted electronic feedbacks, all input signals and measurements were performed in two electrode setups. In Figures 2-3 the input signal was produced with a BioLogic VSP-300 multichannel potentiostat. The voltage and current measurements were conducted with a separate channel from the same potentiostat. Voltage measurements were taken with a sampling time of 200 µs and current measurements were taken with a sampling time of 400 µs. All the potentiostat channels were in floating mode. The RBIP performance discussed in Figure 2 was characterized using the following procedures. First, V_{in} was set to 0 V for 30 s. Next, the ratchet signal was introduced for 90 s. Finally, V_{in} was set to 0 V for another 60 s. The ratchet induced voltage $\Delta\bar{V}_{out}$ was calculated according to $\bar{V}_{out} = \bar{V}_{out,ON} - (\bar{V}_{out,OFF_1} + \bar{V}_{out,OFF_2})/2$ and the ratchet induced current $\Delta\bar{I}_{out}$ was calculated according to $\bar{I}_{out} = \bar{I}_{out,ON} - (\bar{I}_{out,OFF_1} + \bar{I}_{out,OFF_2})/2$. $\bar{V}_{out,ON}$ and $\bar{I}_{out,ON}$ are respectively the voltage and current averaged over the last 30 s of the period in which the input signal was applied. $\bar{V}_{out,OFF_1}$ and $\bar{I}_{out,OFF_1}$ are respectively the voltage and current averaged over the last 15 s in the first (30 s long) period in which V_{in} = 0 V. $\bar{V}_{out,OFF_2}$ and $\bar{I}_{out,OFF_2}$ are respectively the voltage and current averaged over the last 30 s of the second OFF period.

In Figure S9 and Figure S14 the input signal was generated with a HP 3245A universal source. The voltage between the Ag/AgCl wires was measured with an Agilent 34401A multimeter where both instruments shared the same ground. The voltage measurement was conducted with an integration time of 1.67 s to reduce the output signal oscillations and obtain only the net averaged voltage. The response to every input signal was measured for 300 s after which the input was set to 0 V for 300 s. $\bar{V}_{out,ON}$, $\bar{V}_{out,OFF_1}$ and $\bar{V}_{out,OFF_2}$ were averaged over the last 150 s of every period.

In Figure 1 the input signal was supplied with a Keysight 33510B waveform generator and voltages were measured with Keysight 34465A multimeters. The response to every input signal was measured for 60 s after which the input was set to 0 V for 60 s. The voltage V_L was measured between the left gold contact and the adjacent Ag/AgCl wire, and V_R was calculated using equation (1). In Figure 1f,g, the mean temporal signals $V_L(t)$, and $V_R(t)$ were found by obtaining the mean responses out of 300 periods. Figure S3 shows an example of the measured signal and the $\Delta\bar{V}_{out}$ calculation.

In the experiment described in Figure 3b, the duration of the first set of ON cycles was 5 min after which the ratchet was turned OFF (V_{in} = 0 V) for 30 s. In later sets, the ratchet ON duration was 30 min and the duration of the OFF interval was 90 s. To reduce noise, in the long duration ratchet OFF period (black curve in Figure 3b) every 20 data points were averaged together. V_{out} was measured during every ratchet OFF interval and the auxiliary electrodes were not shunted during this time.

In some samples, input of a constant bias higher than ±300 mV resulted in a constant, non-negligible V_{out}. This may suggest Faradaic reactivity, which was followed by degradation in the RBIP performance

for some samples. In other samples, non-zero V_{out} under a constant bias was attributed to blocked pores.

Acknowledgments

RK acknowledges the U.S. National Science Foundation Graduate Research Fellowship Program (DGE-1321846). AH acknowledges the support of the Boris Mints Institute. EJH acknowledges a Graduate Assistance in Areas of National Need (GAANN) Fellowship. CM acknowledges the gracious support for summer research at UC Irvine from Research Corporation for Science Advancement through a Cottrell Scholars Collaborative (Award #27512) awarded to SA and the UCI Vice Provost for Teaching and Learning. JWA was supported by the Joint Center for Artificial Photosynthesis, a DOE Energy Innovation Hub, supported through the Office of Science of the U.S. Department of Energy under Award No. DE-SC0004993. SA acknowledges the support of the Gordon and Betty Moore Foundation under a Moore Inventor Fellowship (GBMF grant #5641) and The Beall Family Foundation (UCI Beall Innovation Award). SA also acknowledges the Phase I Centers for Chemical Innovation (CCI) Program in the U.S. National Science Foundation Division of Chemistry under Grant CHE-2221599 for supporting collaborative student exchanges with the Sa Group at the University of Massachusetts Boston, as well as revisions to the initial manuscript submission.GS thanks the Azrieli Foundation for financial support within the Azrieli Fellows program. This work is partially funded by the European Union (ERC, ESIP-RM, 101039804). Views and opinions expressed are however those of the author(s) only and do not necessarily reflect those of the European Union or the European Research Council Executive Agency. Neither the European Union nor the granting authority can be held responsible for them. We would also like to acknowledge Prof. Reg Penner for allowing us to work with his group members and use their thermal evaporator for the fabrication of some of the RBIPs.

Conflict of Interest

GS, JWA, FMT, and SA filed patent applications US 16/907,076 and US 17/125,341 for ratchet-based ion pumping membrane systems. There are no other conflicts of interest to declare.

Author contributions

GS, JWA and SA conceptualized this work, RK, AH, EJH, CM, DL and GS conducted the investigation, AH, SA and GS designed the methodology, RK, AH EJH, CM and GS conducted the formal analysis and acquired the data, visualizations were designed by EJH, AH, RK, SA and GS, the original draft was written by SA and GS, and all authors contributed to its reviewing and editing. GS and SA supervised the project, GS, SA and FMT administered it, and acquired the funding for it.

References

1. Kedem, O., Lau, B. & Weiss, E. A. How to Drive a Flashing Electron Ratchet to Maximize Current. *Nano Lett.* **17**, 5848–5854 (2017).

2. Kedem, O., Lau, B. & Weiss, E. A. Mechanisms of Symmetry Breaking in a Multidimensional Flashing Particle Ratchet. *ACS Nano* **11**, 7148–7155 (2017).

3. Kedem, O., Lau, B., Ratner, M. A. & Weiss, E. A. Light-responsive organic flashing electron ratchet.

Proc. Natl. Acad. Sci. **114**, 8698–8703 (2017).

4. Roeling, E. M. *et al.* Organic electronic ratchets doing work. *Nat. Mater.* **10**, 51–55 (2011).

5. Kedem, O., Lau, B. & Weiss, E. A. How to Drive a Flashing Electron Ratchet to Maximize Current. *Nano Lett.* **17**, 5848–5854 (2017).

6. Tarlie, M. B. & Astumian, R. D. Optimal modulation of a Brownian ratchet and enhanced sensitivity to a weak external force. *Proc. Natl. Acad. Sci.* **95**, 2039–2043 (2002).

7. Parrondo, J. M. R., Blanco, J. M., Cao, F. J. & Brito, R. Efficiency of Brownian motors. *Europhys. Lett.* **43**, 248–254 (1998).

8. Jung, P., Kissner, J. G. & Hänggi, P. Regular and chaotic transport in asymmetric periodic potentials: Inertia ratchets. *Phys. Rev. Lett.* **76**, 3436–3439 (1996).

9. Rozenbaum, V. M. High-temperature brownian motors: Deterministic and stochastic fluctuations of a periodic potential. *JETP Lett.* **88**, 342–346 (2008).

10. Lau, B., Kedem, O., Schwabacher, J., Kwasnieski, D. & Weiss, E. A. An introduction to ratchets in chemistry and biology. *Mater. Horizons* **4**, 310–318 (2017).

11. Squires, T. M. Induced-charge electrokinetics : fundamental challenges and opportunities. *Lab Chip* 2477–2483 (2009) doi:10.1039/b906909g.

12. Schwemmer, C., Fringes, S., Duerig, U., Ryu, Y. K. & Knoll, A. W. Experimental Observation of Current Reversal in a Rocking Brownian Motor. *Phys. Rev. Lett.* **121**, 104102 (2018).

13. Nicollier, P. *et al.* Nanometer-Scale-Resolution Multichannel Separation of Spherical Particles in a Rocking Ratchet with Increasing Barrier Heights. *Phys. Rev. Appl.* **15**, 034006 (2021).

14. Skaug, M. J., Schwemmer, C., Fringes, S., Rawlings, C. D. & Knoll, A. W. Nanofluidic rocking Brownian motors. *Science (80-.).* **359**, 1505–1508 (2018).

15. Słapik, A., Łuczka, J., Hänggi, P. & Spiechowicz, J. Tunable Mass Separation via Negative Mobility. *Physical Review Letters* vol. 122 (2019).

16. Motz, T., Schmid, G., Hänggi, P., Reguera, D. & Rubí, J. M. Optimizing the performance of the entropic splitter for particle separation. *J. Chem. Phys.* **141**, 074104 (2014).

17. Reguera, D. *et al.* Entropic splitter for particle separation. *Phys. Rev. Lett.* **108**, 1–5 (2012).

18. Yang, B., Long, F. & Mei, D. C. Negative mobility and multiple current reversals induced by colored thermal fluctuation in an asymmetric periodic potential. *Eur. Phys. J. B* **85**, 2–7 (2012).

19. Siwy, Z. & Fuliński, A. A nanodevice for rectification and pumping ions. *Am. J. Phys.* **72**, 567–574 (2004).

20. Siwy, Z. & Fuliński, A. Fabrication of a Synthetic Nanopore Ion Pump. *Phys. Rev. Lett.* **89**, 4–7 (2002).

21. Wu, X., Ramiah Rajasekaran, P. & Martin, C. R. An Alternating Current Electroosmotic Pump Based on Conical Nanopore Membranes. *ACS Nano* **10**, 4637–4643 (2016).

22. Herman, A., Ager, J. W., Ardo, S. & Segev, G. Ratchet-Based Ion Pumps for Selective Ion

Separations. *PRX Energy* **2**, 023001 (2023).

23. Bazant, M. Z., Thornton, K. & Ajdari, A. Diffuse-charge dynamics in electrochemical systems. *Phys. Rev. E* **70**, 021506 (2004).

24. Kerner, Z. & Pajkossy, T. On the origin of capacitance dispersion of rough electrodes. *Electrochim. Acta* **46**, 207–211 (2000).

25. Pajkossy, T. Impedance spectroscopy at interfaces of metals and aqueous solutions — Surface roughness, CPE and related issues. *Solid State Ionics* **176**, 1997–2003 (2005).

26. Pajkossy, T. Impedance of rough capacitive electrodes. *J. Electroanal. Chem.* **364**, 111–125 (1994).

27. Lasia, A. Electrochemical Impedance Spectroscopy and its Applications. in *Modern Aspects of Electrochemistry* 143–248 (Kluwer Academic Publishers). doi:10.1007/0-306-46916-2_2.

28. Galama, A. H., Post, J. W., Hamelers, H. V. M., Nikonenko, V. V. & Biesheuvel, P. M. On the origin of the membrane potential arising across densely charged ion exchange membranes: How well does the teorell-meyer-sievers theory work? *J. Membr. Sci. Res.* **2**, 128–140 (2016).

29. Marbach, S., Kavokine, N. & Bocquet, L. Resonant osmosis across active switchable membranes. *J. Chem. Phys.* **152**, (2020).

30. Herman, A. & Segev, G. Ambipolar Ion Pumping with Ratchet Driven Active Membranes. *Phys. Rev. Appl.* **21**, 034056 (2024).

31. Vega, V. *et al.* Diffusive transport through surface functionalized nanoporous alumina membranes by atomic layer deposition of metal oxides. *J. Ind. Eng. Chem.* **52**, 66–72 (2017).

Supporting information for A nanoporous capacitive electrochemical ratchet for continuous ion separations

Rylan Kautz[1], Alon Herman[2], Ethan J. Heffernan[1], Camila Muñetón[3,4], David Larson[5,6], Joel W. Ager III[5,6,7,8], Francesca M. Toma[5,6,9], Shane Ardo[1,3,10]* and Gideon Segev[2,5,6]**

[1]Department of Materials Science & Engineering, University of California Irvine, Irvine, CA 92697, USA
[2]School of Electrical Engineering, Tel Aviv University, Tel Aviv 6997801, Israel
[3]Department of Chemistry, University of California Irvine, Irvine, CA 92697, USA
[4]Department of Chemistry, University of Massachusetts Boston, Boston, MA 02125 USA
[5]Chemical Sciences Division, Lawrence Berkeley National Lab, Berkeley, CA 94720, USA
[6]Joint Center for Artificial Photosynthesis, Lawrence Berkeley National Lab, Berkeley, CA 94720, USA
[7]Materials Sciences Division, Lawrence Berkeley National Lab, Berkeley, CA 94720, USA
[8]Department of Materials Science and Engineering, University of California Berkeley, Berkeley, CA 94720, USA
[9]Institute of Functional Materials for Sustainability, Helmholtz Zentrum Hereon, Teltow, 14513, DE
[10]Department of Chemical & Biomolecular Engineering, University of California Irvine, Irvine, CA 92697, USA

*Email: ardo@uci.edu
**Email: gideons1@tauex.tau.ac.il

Sample assembly

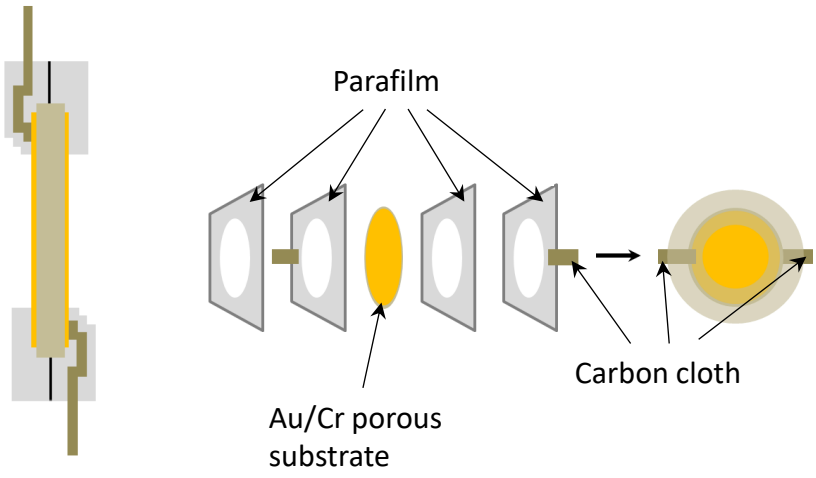

Figure S1: Schematic illustration of an RBIP sample assembly in test setup.

Duty cycle sweep additional data

Figure S2a-c show respectively the fitted effective amplitude, $V_i - V_f$, the final potential, V_f , and the fit R^2 as a function of the input signal duty cycle obtained from the data presented in Figure 1f-g. Figure S2d shows the measured signals as well as the signals obtained by inserting the fitted values into equations 3 and 1. The charging/discharging response to a large voltage step is non-linear with the potential as it includes the fast relaxation of the electrochemical double layer, and the slower relaxation of other ionic processes.[1] As a result, the time constants describing the charging and discharging of the surfaces increase with the duration of the voltage step (Figure 1h). Furthermore, the fitted curves in Figure 1f-g do not account for the fast processes and consistently underestimate the temporal change near $t = 0$ and $t = d_c T$. Figure S2e shows the net output voltage, $\Delta\bar{V}_{out}$, obtained from the measurements (Figure 1i) and by integrating the fitted data from Figure S2d. The good agreement between the measured and the output obtained with the fitted data implies that the performance of the RBIP can be described with four time constants (charging and discharging each of the surfaces), and that the contribution of the faster processes at $t = 0$ and $t = d_c T$ is small.

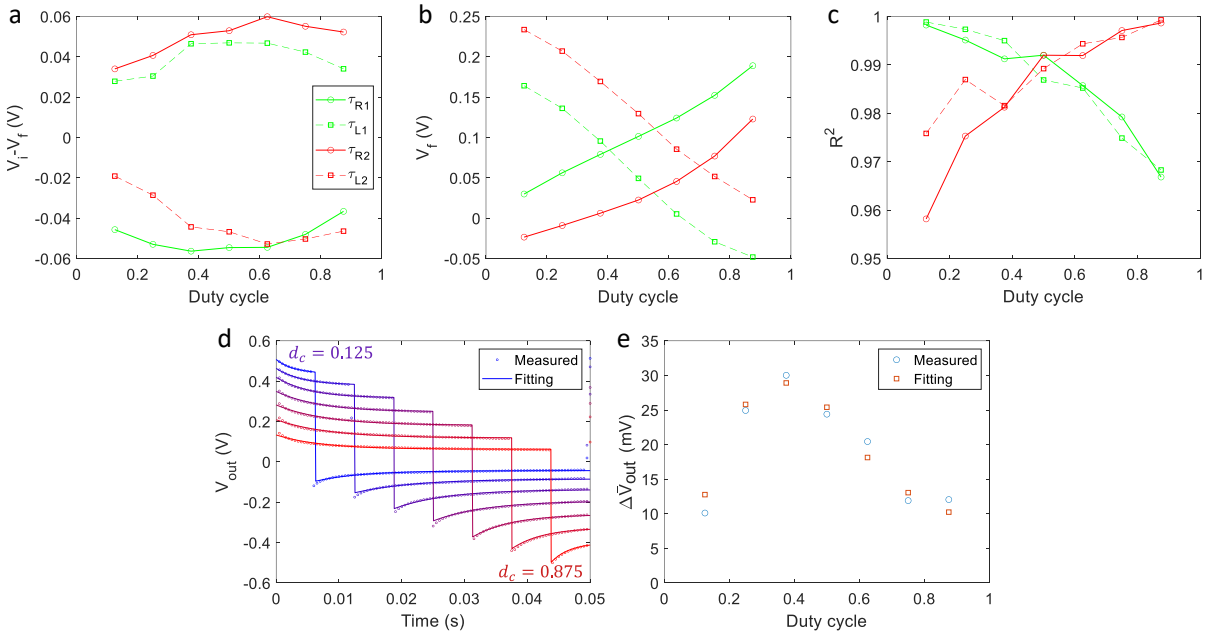

Figure S2: the parameters obtained from the fitting process. (a) The fitted effective amplitude of the input signal $V_i - V_f$, (b) the final potential, V_f, and (c) the fit R^2 as a function of the input signal duty cycle. The color coding is as in (a). (d) the measured averaged V_{out} and V_{out} obtained from the fitted parameters and equations 1-3. (e) the measured ratchet voltage output and the output calculated with the fitted parameters.

Figure S3a shows the raw data measured during the experiment described in figure 1 (the periodic signals cannot be resolved from Figure S3a because of the long duration of the experiment. This data is presented to clarify how the analysis is carried out). The grey shaded areas mark the times when the ratchet was OFF, and the white regions mark the times when the ratchet was ON. The input signal duty cycle is indicated near the top of every white region. The black curve is the measured voltage. $V_{out,ON}$ (light blue) is the voltage measured when the ratchet was ON and that was later used to calculate the time averaged voltage $\bar{V}_{out,ON}$ as described in the methods section. The time averaged voltage, $\bar{V}_{out,ON}$, for every duty cycle is indicated with markers. $\bar{V}_{out,OFF}$ (not shown Figure S3a) is the temporal average of V_{out} when the

ratchet was OFF and was obtained by averaging the red areas in Figure S3a. Figure S3b shows the same measurement as in Figure S3a focusing on a short timespan with duty cycle of 0.5, allowing the recorded signal to be observed. Figure S3c shows the time averaged voltages $\bar{V}_{out,ON}$ and $\bar{V}_{out,OFF}$ and how the ratchet voltage output $\Delta\bar{V}_{out}$ is calculated: $\Delta\bar{V}_{out} = \bar{V}_{out,ON} - (\bar{V}_{out,OFF,1} + \bar{V}_{out,OFF,2})/2$.

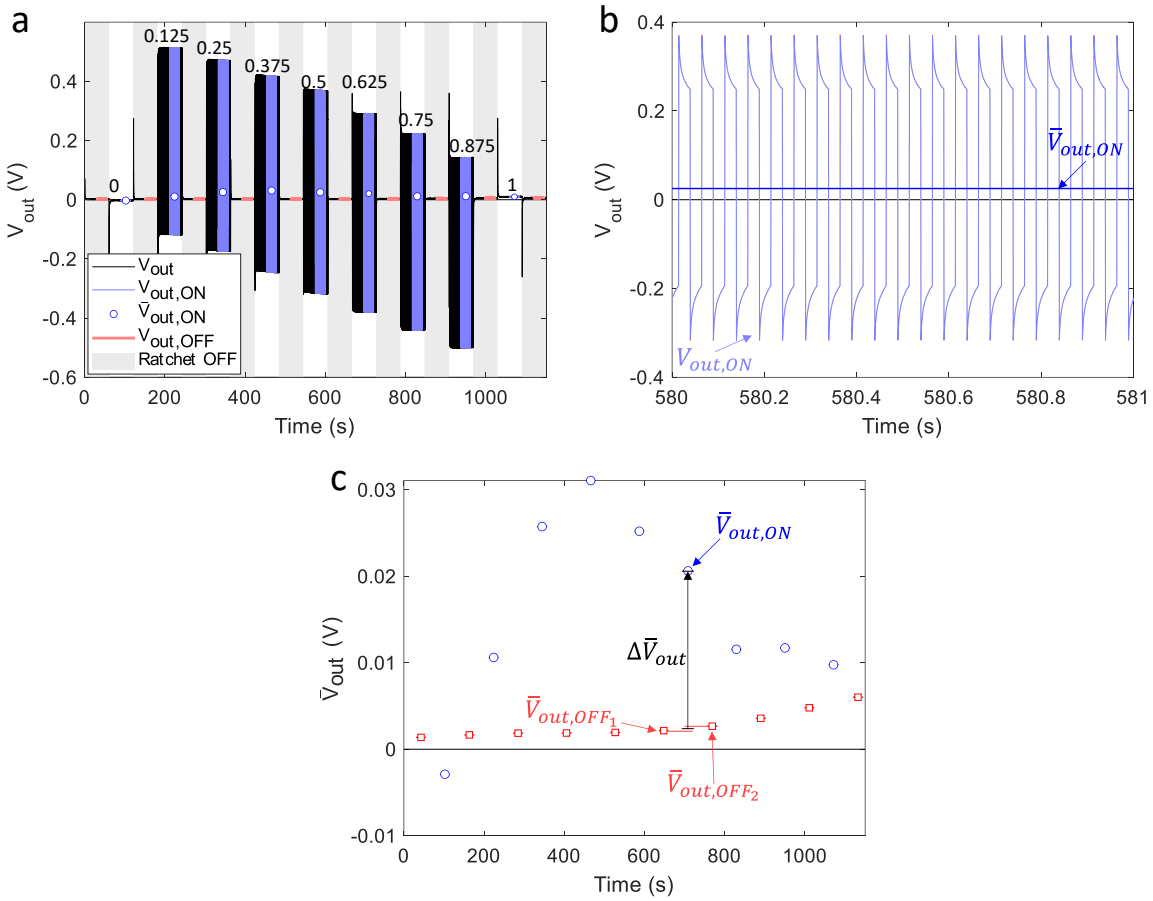

Figure S3: $\Delta\bar{V}_{out}$ calculation, (a) The raw data recorded in the experiment described in Figure 1, and the ratchet output calculation. The grey shaded areas mark the time when the ratchet was OFF, and the white regions mark the time when the ratchet was ON. The black curve is the measured voltage. The numbers indicate the duty cycle of the input signal. (b) An example of $V_{out,ON}$ and $\bar{V}_{out,ON}$ within a short timespan with duty cycle of 0.5, which allows observing the recorded signal. (c) The time averaged voltages $\bar{V}_{out,ON}$ and $\bar{V}_{out,OFF}$ and the ratchet voltage output $\Delta\bar{V}_{out}$ calculation: $\Delta\bar{V}_{out} = \bar{V}_{out,ON} - (\bar{V}_{out,OFF,1} + \bar{V}_{out,OFF,2})/2$.

Time constants extraction- frequency sweep

The sample analyzed in Figure 1f,g was also measured at various input signal frequencies. The duty cycle is 0.5, and the amplitude is V_a = 0.7 V. The electrolyte is 0.2 mM NaCl aqueous solution. All other parameters are as described in Figure 1. Figure S4a-c show respectively the average temporal responses of V_L, V_R, and V_{out}. For clarity, the time for every signal was normalized by its period. The input signal frequency is indicated by the color bar. For the lowest frequency (0.1 Hz) three temporal periods were averaged to obtain the average response, for a frequency of 0.2 Hz, 8 periods were averaged, and for higher frequencies at least 15 periods were averaged. The solid lines show the best exponential fit to the

measured data. Figure S5a shows the extracted time constants of the measured signals for the two parts of the input signal ($0<t<d_cT$, and $d_cT<t<T$). The time constants for all signals drop significantly with the input signal frequency demonstrating the frequency dispersion. Differences between the time constants for the two parts of the input signals are also observed. Figure S5b-c shows respectively the extracted values of V_i-V_f and V_f for each of the signals. Because the effective time constants increase as the frequency decreases, V_f reaches the applied voltage only for very low frequencies. As a result, the effective amplitude of the potential modulation at the ratchet contacts, $V_i - V_f$, also decreases with frequency. This implies that at high frequencies the voltage V_L and V_R alternate according to an effective input signal with an amplitude that is smaller than V_a, potentially reducing the output of the device.

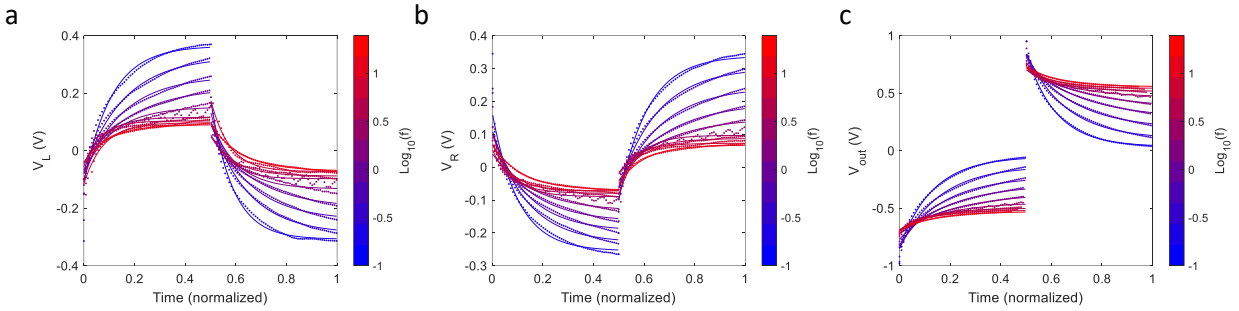

Figure S4: (a-c) The averaged responses of $V_L(t)$, $V_R(t)$ and $V_{out}(t)$ respectively for various input signal frequencies. The sample is as in Figure 1. The duty cycle is 0.5, and the amplitude is V_a = 0.7 V. The electrolyte is 0.2 mM NaCl aqueous solution. For each signal, the time was normalized by the input signal temporal period. The color bar indicates the input signal frequency. The symbols mark the measured signals, and the solid lines are the exponential fit. The plotted measured signals were under-sampled for visualization purposes.

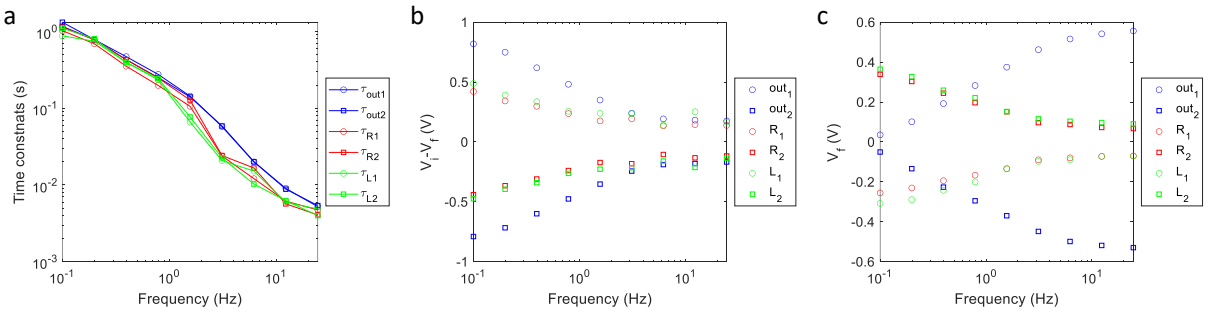

Figure S5: (a) Extracted time constants, (b) the fitted effective amplitude $V_i - V_f$, and (c) Vf for the signals shown in Figure S4.

The average responses for the data presented in Figure 2

Figure S6a-e shows the measured average response $V_{out}(t)$ for various duty cycles and frequencies of 1, 5, 10, 25, 50 Hz in (a-e) respectively. Each output is the averaged response of at least 30 temporal periods. The sample is as in Figure 2, the electrolyte is 1 mM HCl aqueous solution, the RBIP pore diameter is 40 nm, the active area of the membrane is A = 0.32 cm^2, and the input signal amplitude, V_a, is 0.3 V. For frequencies of 125 and 250 Hz there were not enough measured data points per period to carry out the fitting process properly.

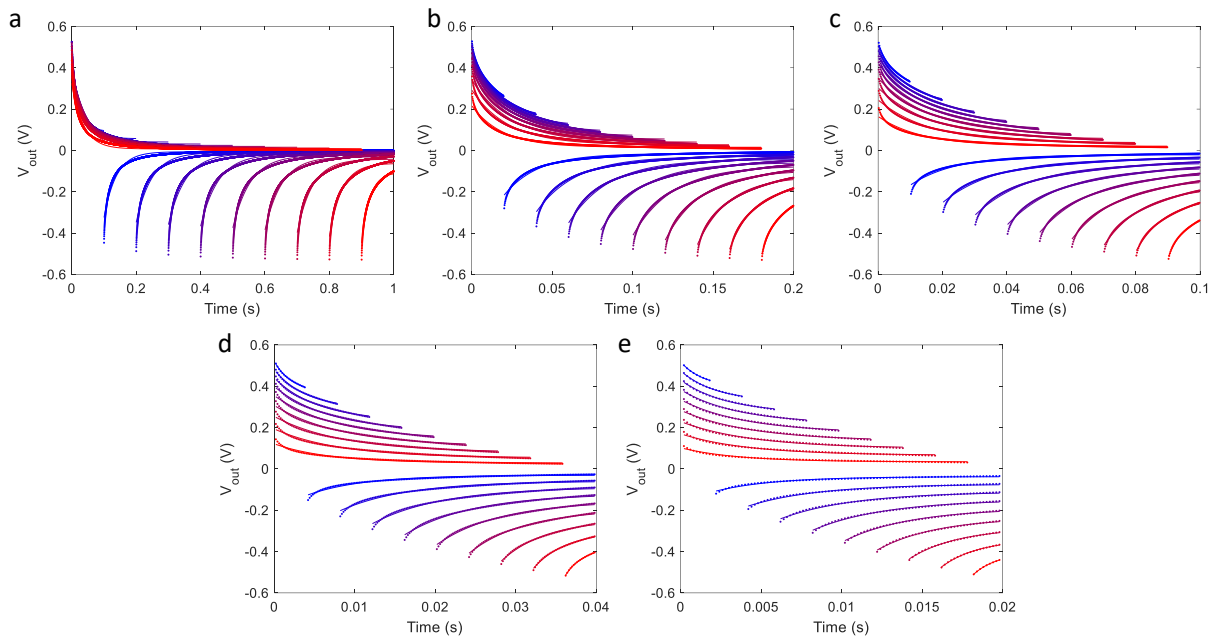

Figure S6: Measured $V_{out}(t)$ for various duty cycles (dots) and the best fit to single exponential functions. The color coding matches the input signal duty cycle. The input signal frequencies are 1, 5, 10, 25, 50 Hz in (a-e) respectively. Each output is the averaged response of at least 30 temporal periods. The electrolyte is 1 mM HCl aqueous solution, the RBIP pore diameter is 40 nm, the active area of the membrane is A = 0.32 cm², and the input signal amplitude, V_a, is 0.3 V.

Figure S7a shows the average temporal response of I_{out}(t). The RBIP and signal parameters are as in Figure 2a. The measured current is normalized by the RBIP active area (A = 0.32 cm^2), and the time is normalized by the temporal period of every signal. The response for other duty cycles and the best fit to exponential functions are shown in Figure S6. Figure S7b shows the time constants obtained from I_{out}(t). As in the time constants obtained from the voltage measurement, the current time constants vary significantly with frequency and duty cycle, and the time constants of the first part of every period are close to those of the second part of the period flipped with respect to a duty cycle of 0.5. The color coding is as in Figure S5a. The time constants for frequencies of 125 and 250 Hz were not extracted because there were not enough measured data points per period to carry out the fitting process properly.

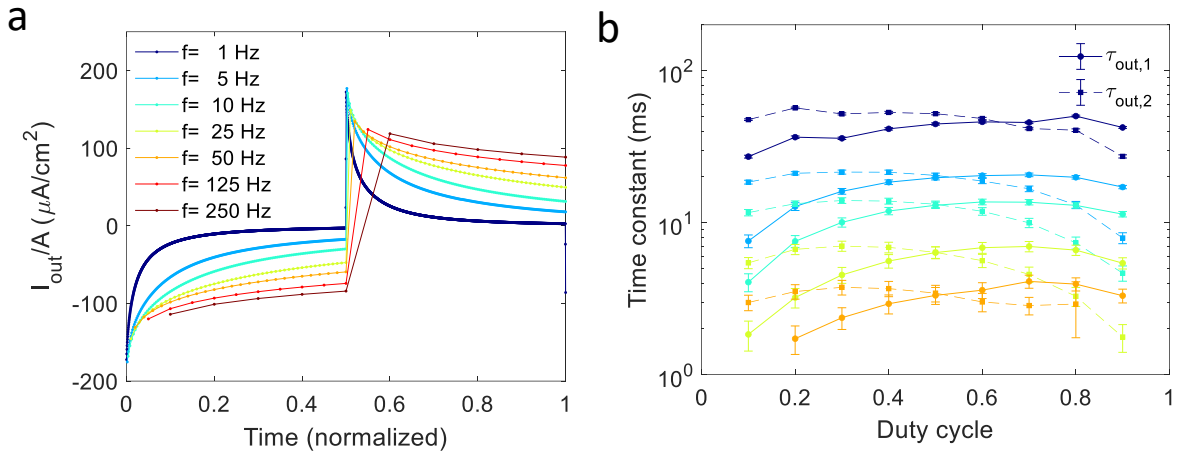

Figure S7: (a) Current density, I_{out}/A, as a function of time for several input signal frequencies and a duty cycle of 0.5. (b) Time constants of I_{out} for several input signal frequencies and duty cycles. The sample is as in Figure 2, the RBIP pore diameter is 40 nm, the active area of the membrane is A = 0.32 cm^2, the electrolyte is 1 mM HCl aqueous solution, and the input signal amplitude, V_a, is 0.3 V.

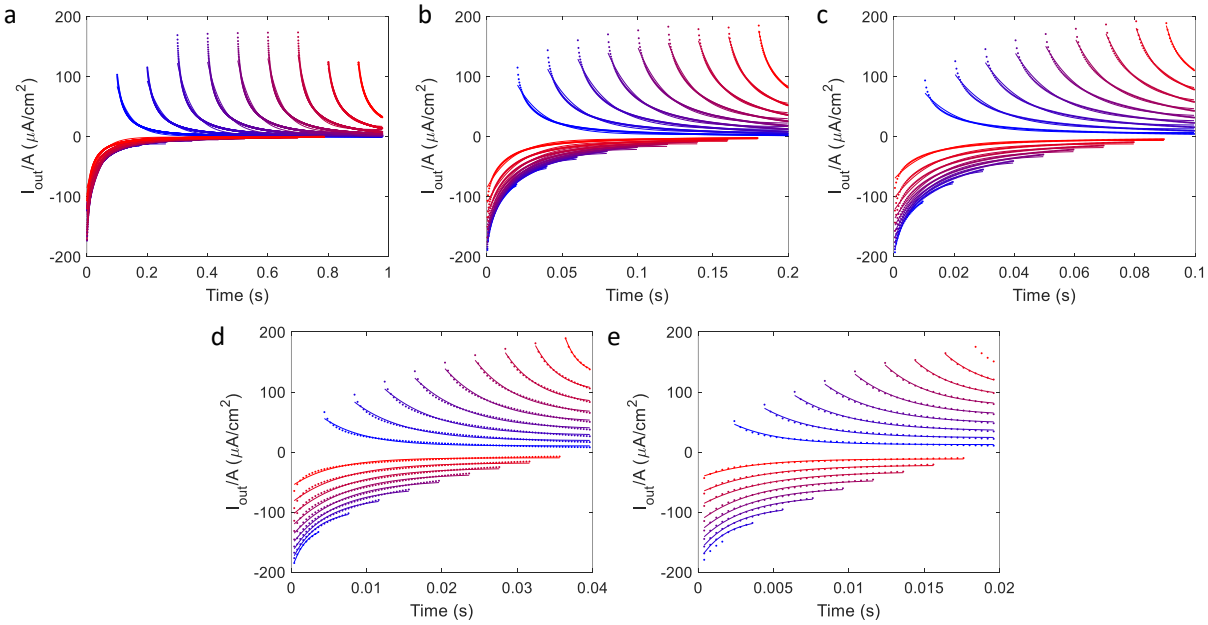

Figure S8: Measured $I_{out}(t)$ for various duty cycles (dots) and the best fit to single exponential functions. The color coding matches the input signal duty cycle. The input signal frequencies are 1, 5, 10, 25, 50 Hz in (a-e) respectively. Each output is the averaged response of at least 30 temporal periods.

Additional results and methods

RBIP with a pore diameter of 40 nm in KCl aqueous electrolyte

Here we have tested the performance of an RBIP fabricated on AAO wafers with 40 nm diameter pores. The wafers were air annealed for 11 h at 650 °C. The contacts were deposited with electron beam evaporation of 10 nm of titanium and 40 nm of gold (planar equivalent). For the results presented in this section, unless stated otherwise, the input electric signal $V_{\text{in}}(t)$ is a rectangular wave at a frequency of 100 Hz, and the amplitude, V_a, is 0.2 V. The ratchet input signal, V_{in}, was applied with an HP 3245A universal source and the voltage between the Ag/AgCl wires was measured with an Agilent 34401A multimeter, where both instruments shared the same ground. The voltage measurement was conducted with an integration time of 1.67 s to reduce the output signal oscillations and obtain only the net time averaged voltage, $\bar{V}_{out}$. The response to every input signal was measured for 5 min after which the input was set to 0 V for 5 min. Figure S9a shows the recorded voltage for duty cycles between 5% and 100% (the duty cycle is the portion of the time in every period where the voltage is at its high value. The input signal duty cycle is marked next to the output curve in Figure S9a).

Once a ratchet signal commences, V_{out} quickly builds up to a level determined by the duty cycle. The ratchet-induced voltage reaches its largest values for duty cycles close to 50%, i.e., a temporally averaged input voltage of 0 V. For a duty cycle of 100%, which is the response to a voltage step from 0 V to 0.2 V, the voltage signal shows the well expected, fast capacitive charging behavior corresponding to polarization of the metal contacts. However, unlike the response to a duty cycle of 100%, for a duty cycle of 95% (a temporal average input voltage of 0.19 V), a ratchet action is observed and $V_{out}(t)$ has a negative sign with a much slower decay time. This provides a simple distinction between steady-state ratchet-driven transport and capacitive charging–discharging behavior.

To estimate the ratchet output voltage, the measured voltage was averaged over the last 2.5 min of every cycle and the difference between the ratchet ON and ratchet OFF average voltages was calculated. Figure S9b shows the ratchet time averaged output voltage, $\Delta\bar{V}_{out}$, as a function of the input signal amplitude, V_a, for 1 mM and 10 mM KCl aqueous solutions. More details on how $\Delta\bar{V}_{out}$ is calculated can be found in the Methods section. The input signal was an unbiased square wave with a frequency of 100 Hz, and a duty cycle of 50%. For the 1 mM KCl solution, a noticeable ratchet output is visible for ratchet signals with an amplitude as small as 0.05 V. This extremely low voltage threshold provides a clear distinction between ratchet-induced ion transport, where the voltage threshold is about *2kT* (*k* is the Boltzmann constant (1.381×10^{-23} J K^{-1}) and *T* is the temperature (K)), and ion transport induced by chemical reactions where the threshold bias is determined by the Gibbs free energy and the reaction overpotentials. The ratchet output is significantly smaller with the 10 mM KCl solution. This is an expected result, because at a higher ion concentration potential screening is more significant, and as a result the center of the pore is less affected by the input signal and can serve as a shunt for back-diffusing ions. Figure S9c-d shows the ratchet output voltage as a function of the frequency and duty cycle in 1 mM and 10 mM KCl, respectively. Since ratchet systems have no long-term output when a DC voltage is applied, the RBIP output voltage is close to 0 V for duty cycles near 0% and 100%. Similarly, at low frequencies, the RBIP fully charges and discharges the double layers, which is similar to operation under DC bias. Thus, the output is near 0 V at low frequencies as well. As a result, the RBIP shows a significant output only when operated with duty cycles near 50% and at input signal periods that are close to the characteristic charging–discharging time constant of the RBIP. When the input signal period is significantly shorter than the RBIP charging and discharging time constants the output again goes to 0 V.

The output of the ratchet was measured when switching the leads connected to the RBIP contacts, and the leads of the Ag/AgCl wires (used to measure V_{out}). Figure S10a shows the measurement setup and Figure S10b shows $\bar{V}_{out}$ as a function of the duty cycle for every measurement configuration. According to equation (2) in the main text, $V_{in}(t, d_c) = -V_{in}(t, 1 - d_c)$. Thus, switching the positive and negative leads for V_{in} ('Ratchet Switch' in Figure S10a-b) resulted in $\bar{V}_{out}$ values that were reflected around 50% duty cycle such that $\bar{V}_{out,1}(d_c) = \bar{V}_{out,2}(1 - d_c)$; switching the positive and negative leads for $\bar{V}_{out}$ ('Ag/AgCl Switch' in Figure S10a-b) resulted in oppositely-signed values for $\bar{V}_{out}$, such that $\bar{V}_{out,1}(d_c) = -\bar{V}_{out,2}(d_c)$.

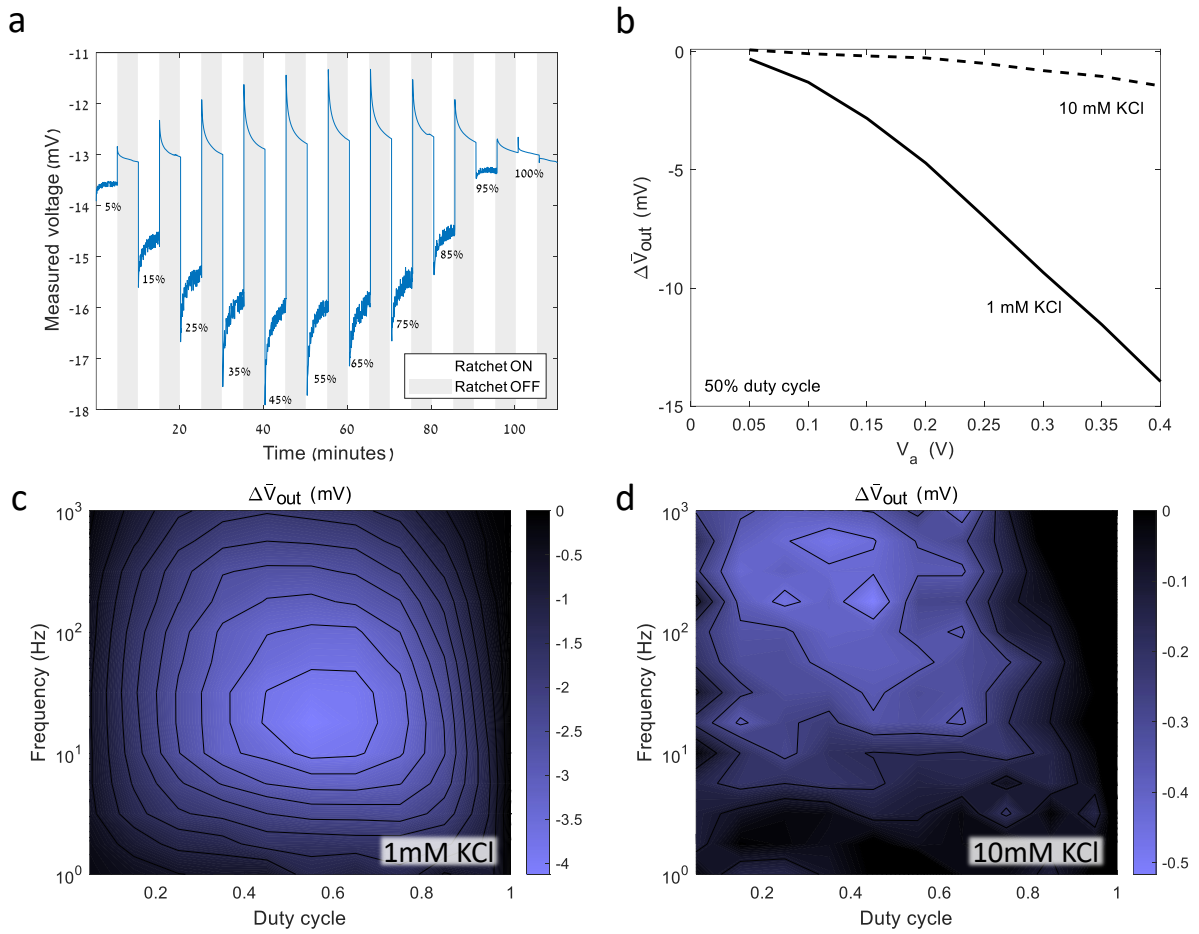

Figure S9: The output of a RBIP sample with 40 nm pores. (a) Measured output voltage, V_{out}, for an input signal with various duty cycles. The input signal is a rectangular wave with V_a of 0.2 V, a frequency of 100 Hz, and the electrolyte is 1 mM KCl aqueous solution. (b) The ratchet output voltage, $\bar{V}_{out}$, as a function of the input signal amplitude, the frequency is 100 Hz, and the duty cycle is 50%. (c,d) the ratchet output voltage as a function of the input signal frequency and duty cycle. The electrolyte is 1 mM KCl aqueous solution (c), and 10 mM KCl aqueous solution (d).

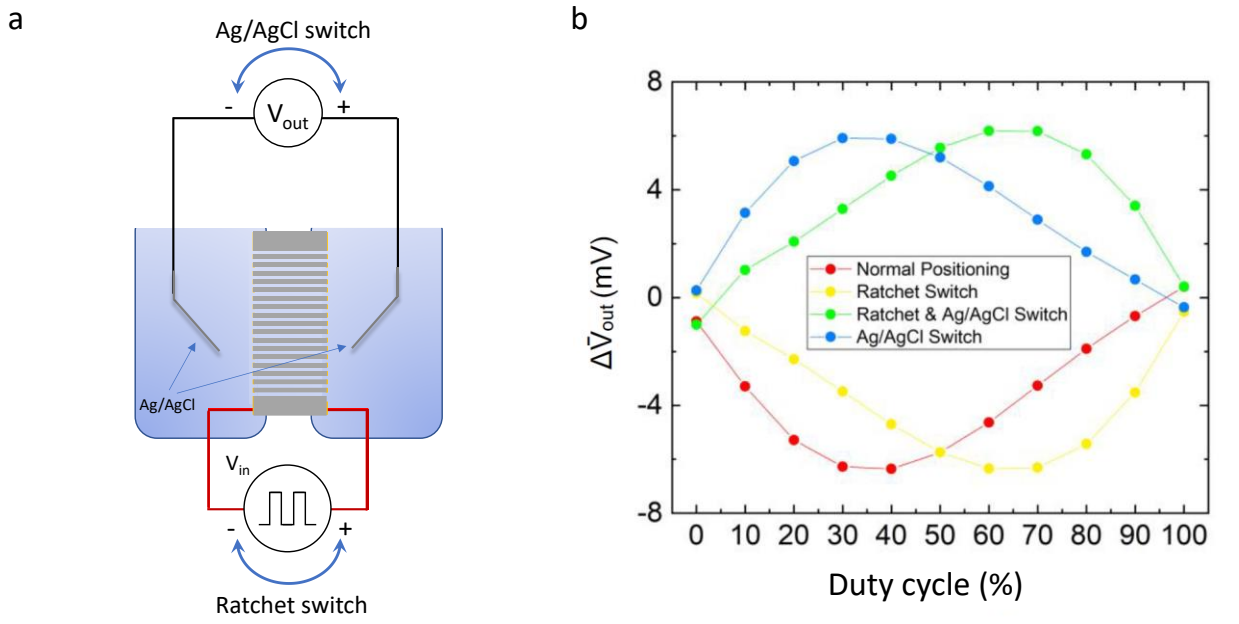

Figure S10: (a) Illustration of the lead-switching experiment, (b) The voltage output of an RBIP, $\Delta\bar{V}_{out}$, when switching the input signal leads, and the leads for the Ag/AgCl voltage-sensing leads. The input signal frequency is 50 Hz and the electrolyte is 1 mM HCl aqueous solution. All other RBIP and input signal parameters are in as in Fig 2.

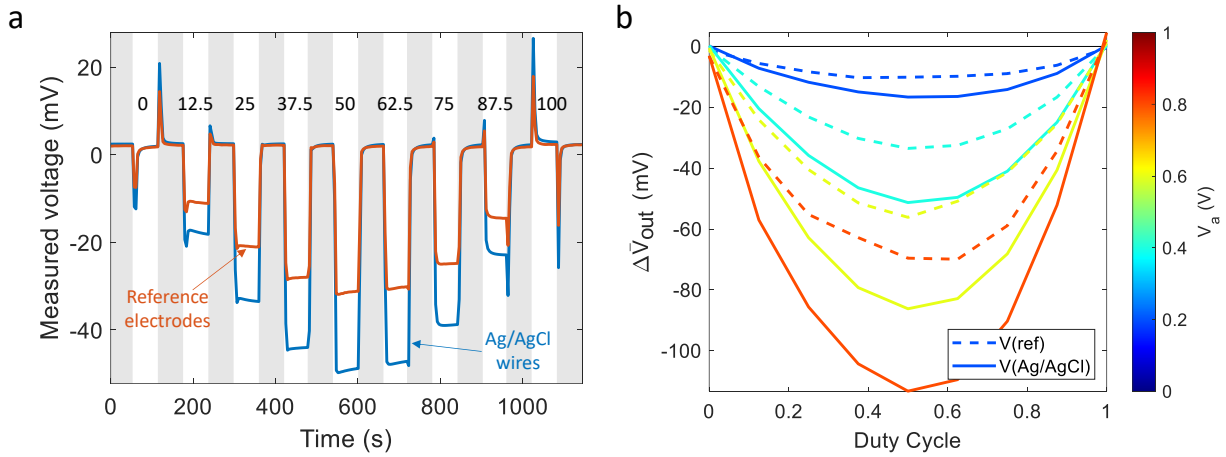

Figure S11: (a) Voltage output, $\bar{V}_{out}(t)$, measured between two Ag/AgCl wires and two leak-free reference electrodes (LF-1-45, Innovative Instruments, Inc.). The pore diameter is 40 nm, the electrolyte is 0.2 mM KCl aqueous solution, the signal frequency is 100 Hz, and the amplitude is V_a =0.4 V. The time periods in which the ratchet operated are the bright areas and the shaded areas are time periods in which the input voltage was set to 0 V. The duty cycle (in percent) used is noted next to the curves. (b) The average ratchet output voltage, $\bar{V}_{out}$, as a function of the duty cycle and several input signal amplitudes measured between two leak-free reference electrodes (dashed line) and Ag/AgCl wires (solid line).

Electro-osmosis was shown to be negligible by running the ratchet continuously while observing the level of the solution within each compartment. The experimental setup is as the one described in Figure 3. The ratchet was driven continuously for 16 minutes and 40 seconds with the auxiliary electrodes shunted. Then, the ratchet was turned OFF and V_{out} was measured for 90 seconds. This process was repeated 9

times for a total of nearly 3 hours. The input signal was a square wave with a frequency of 125 Hz, an amplitude of 300mV and a 50% duty cycle. Each compartment was filled with 1.75 mL of 1mM HCl aqueous solution. The RBIP parameters are as in Figure 3. Although the system was operated for 3 hours, no visible change in water level was observed. Figure S12 shows optical photographs of the setup before and after operation. To further demonstrate that the RBIP prevents any water mass transport between the two compartments, this experiment was repeated with a solution height difference introduced between the two compartments. The solution, RBIP and input signal parameters are identical to those in Figure S12 except that one compartment was filled with 2.25 mL of solution and the other with 1.75 mL. The RBIP was operated for 3 hours as described in Figure S12 after which it was operated continuously for another 45 hours. Figure S13(a-c) shows optical images of the setup at the beginning of the experiment, after 24 and 48 hours respectively. No water transport through the membrane was observed during the experiment.

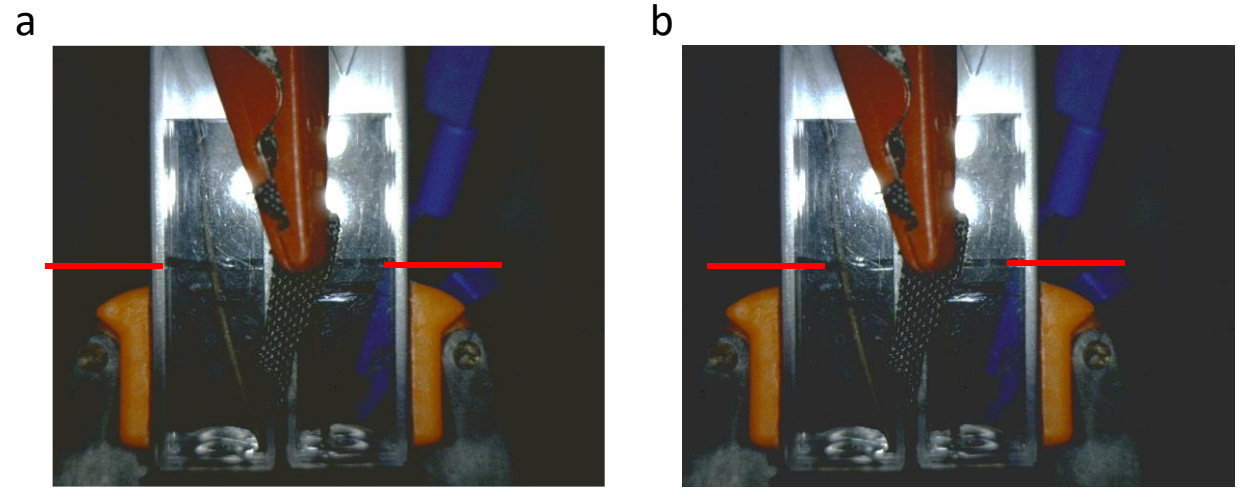

Figure S12: water pumping experiment. Initial water level (a) and after 3 hours of ratchet operation (b). The red lines are guides for the eye indicating the solution level in each compartment. The experimental setup is as the one described in Figure 3. The input signal was a square wave with a frequency of 125 Hz, an amplitude of 300mV and a 50% duty cycle. Each compartment was filled with 1.75 mL of 1mM HCl aqueous solution.

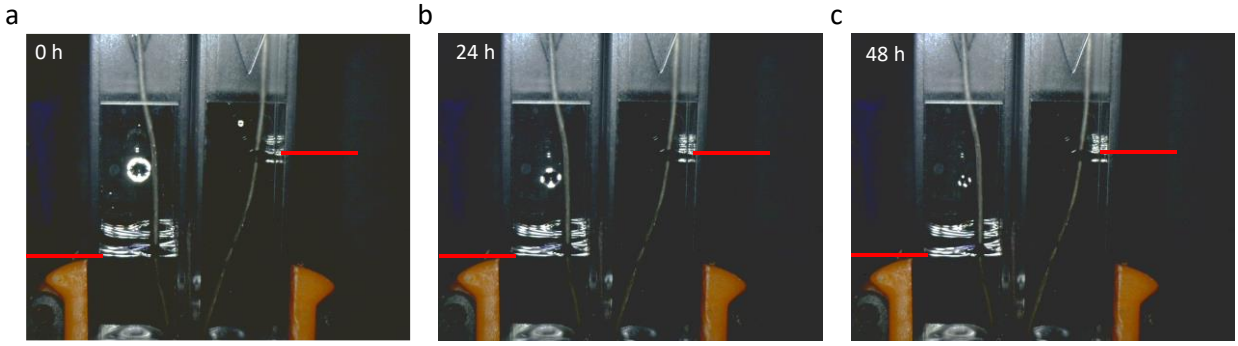

Figure S13: Optical images of the electrochemical cell while an intentional solution level difference is introduced. (a) the initial water level, (b) after 24 hours, (c) after 48 hours. The red lines are guides for the eye indicating the solution level in each compartment. No water transport through the membrane was observed during this time. The solution, RBIP and input signal parameters are identical to those in Figure S12 except that one compartment was filled with 2.25 mL of solution and the other with 1.75 mL.

RBIP with a pore diameter of 20 nm operation in KCl aqueous electrolyte

The same set of measurements as performed in the previous section (using RBIPs with a pore diameter of 40 nm) was repeated using a RBIP constructed on an AAO wafer with 20 nm diameter pores. The sample was air annealed for 11 h at 650 °C and the contacts were deposited by electron beam evaporation of 30 nm of titanium (adhesion layer) and 20 nm of gold (planar equivalent). Figure S14a shows typical data for the measured ratchet signal for an input signal frequency of 100 Hz and duty cycles between 5% and 95%. The electrolyte is 1 mM KCl aqueous solution. The input signal parameters are as in Figure S9a. As discussed above, the ratchet signal was turned ON for 5 min and then the voltage was set to 0 V for 5 min. Unlike the 40 nm pore sample, the response to the ratchet signal does not go to 0 V for duty cycles near 0 and 1. This can be attributed to partial blocking of the pores, caused by their smaller diameter. Further discussion of the effect of blocked pores and other failure modes in RBIP devices can be found in the failure modes section of the supporting information.

Figure S14b shows the 20 nm pore RBIP output, $\Delta\bar{V}_{out}$, as a function of the input signal amplitude, V_a, in 1 mM KCl and 10 mM KCl aqueous solutions. The ratchet output is defined as in Figure S9. The frequency is 100 Hz and the duty cycle is 50%. A noticeable output was recorded for amplitudes as low as 50 mV demonstrating an extremely low voltage threshold. When compared to the 40 nm pore RBIP, the performance of the 20 nm pores RBIP is significantly higher at the higher ionic strength solution. Since in these samples the pore diameter is closer to the Debye length, the electric potential modulation affects a larger portion of the pore. As a result, the decrease in performance with the ionic strength is less pronounced in these RBIPs. Figure S14c-d shows $\Delta\bar{V}_{out}$ as a function of the input signal duty cycle and frequency for 1 mM KCl and 10 mM KCl aqueous solutions, respectively. For 1 mM KCl aqueous solution, the RBIP optimal input signal frequency and duty cycle are 56 Hz and 0.25, respectively, which yield an output of -7.5 mV. For 10 mM KCl solution, the optimal input signal frequency and duty cycle are 316 Hz and 0.35, respectively, and the output is -1.9 mV. The optimal operating frequency increases with the ionic strength and the 20 nm pores RBIP outperforms the 40 nm pores RBIP in higher concentration solutions.

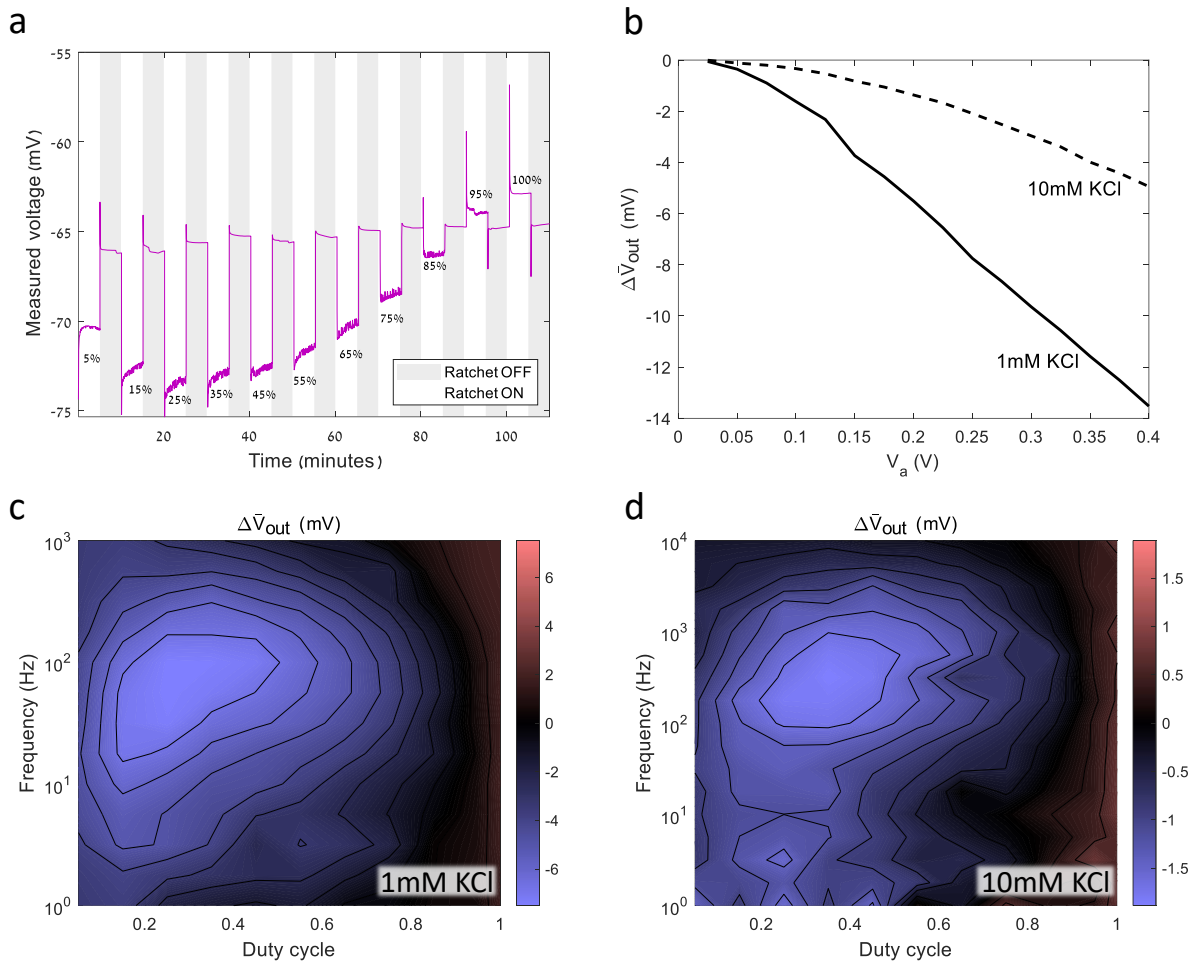

Figure S14: The output of RBIPs with 20 nm pores. (a) Measured voltage for input signals with various duty cycles. The input signal is a square wave with V_a of 0.2 V, the frequency is 100 Hz and the electrolyte is 1 mM KCl aqueous solution. (b) Ratchet output voltage as a function of the input signal amplitude, V_a, the frequency is 100 Hz and the duty cycle is 50%. (c,d) Ratchet output voltage as a function of the input signal frequency and duty cycle. The input signal is a square wave with V_a of 0.2 V. The electrolyte is 1mM KCl aqueous solution (c) and 10mM KCl aqueous solution (d).

Ratchet driven demixing

Figure S15a,b shows $\bar{V}_{out}$ and $\bar{I}_{out}$, respectively, as a funciton of duty cycle for the sample used for the demixing experiment (see Figure 3 in the main text).

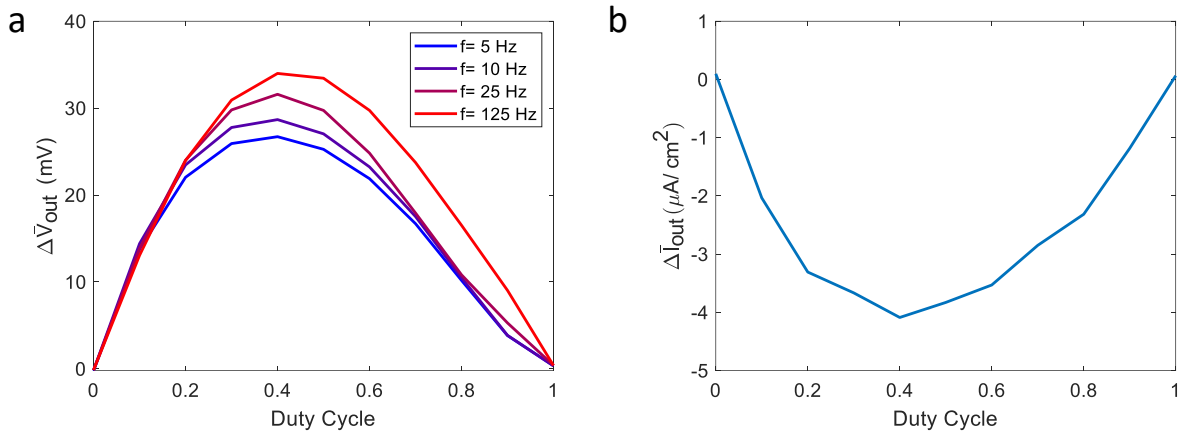

Figure S15: $\Delta\bar{V}_{out}$ (a) and $\Delta\bar{I}_{out}$ (b) as a funciton of duty cycle for the sample used for the demixing experiment discussed in Figure 3 in the main text. The input signal amplitude is V_a =0.3 V, and for (b), the input signal frequency is 125 Hz. The electrolyte is 1 mM HCl aqueous solution.

Figure S16a-c shows the same measurements as in Figure 3(b) focusing on the first three periods in which demixing was demonstrated. The grey shaded areas are times when the ratchet was turned OFF, and the voltage V_{out} was measured. The dashed black curves (long OFF) are the voltages measured while the system was at rest for long durations, and the colored lines (short OFF) are measurements taken in the brief durations between ratchet ON periods. The markers ($\bar{V}_{out}$) are the temporal average of V_{out} in the short OFF intervals. The white areas are the times when the ratchet was ON, and the current between the auxiliary electrodes was measured (red curves). Figure S16d-f shows the voltages measured during the short ratchet OFF periods in (a-c) respectively. Each curve in Figure S16d-f is an expanded view of the voltage measurement shown in Figure S16a-c with the same color. The input signal is a rectangular wave with a duty cycle of 0.5, frequency of 125 Hz, and an amplitude, V_a, of 0.3 V. The electrolyte is 1 mM HCl aqueous solution, the RBIP pore diameter is 40 nm, the active area of the membrane is A = 0.32 cm^2. The red curves in Figure S16a-c are the current densities measured between the auxiliary electrodes (normalized by the ratchet active area). Every data point is obtained by averaging the current over 1 s. The current response can be described in terms of two transient components. The first component is a fast current drop which decays after 5 min. This is the response for pumping ions that back-diffused while the ratchet was turned OFF during voltage measurements. After this initial response, the current magnitude decreases gradually. This slow decrease in current magnitude may be a result of the build-up of a cation concentration gradient as described in the main text. This assumption is supported by measured voltage which saturates in a similar manner.

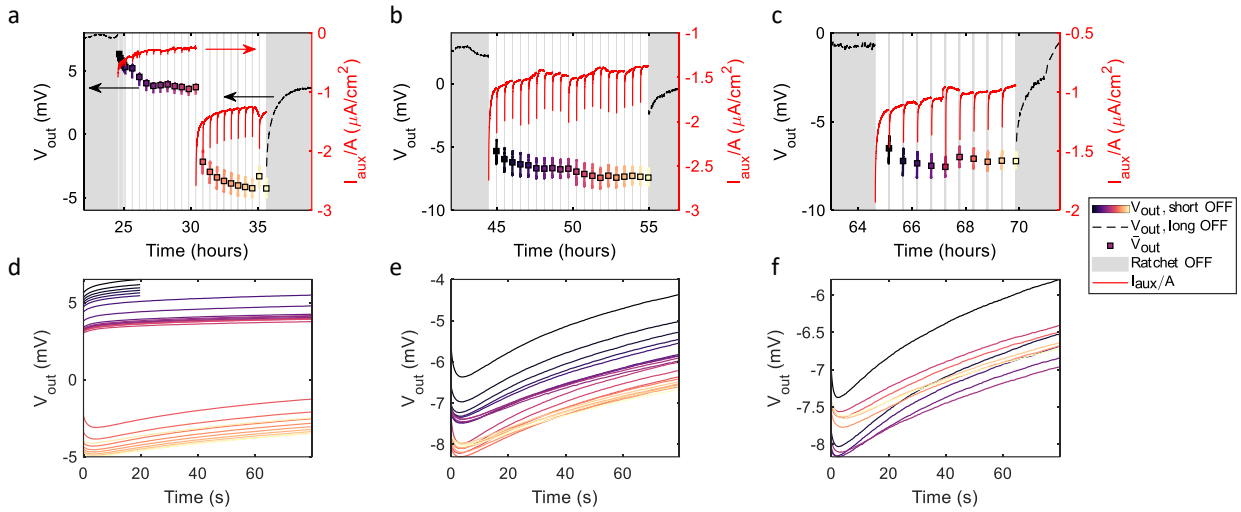

Figure S16: *(a-c) Same measurements as in Figure 3(b) focusing on specific times. The grey shaded areas are times when the ratchet was turned OFF, and the voltage V_{out} was measured. The black curves (V_{out}, long off) are the voltages measured during the prolonged ratchet OFF periods, and the colored lines (V_{out}, short off) are voltages that were measured during the short OFF intervals. The markers are $\bar{V}_{out}$, the temporal average of V_{out}, short off. The red curves are the currents measured between the shorted Ag/AgCl auxiliary electrodes normalized by the RBIP active area. (d-f) Voltages measured during the short ratchet OFF intervals in (a-c) respectively. Each measured curve in (d-f) is an expanded view of the voltage measurement in (a-c) with the same color. The input signal is a rectangular wave with a duty cycle of 0.5, frequency of 125 Hz, and an amplitude, V_a, of 0.3 V. The electrolyte is 1 mM HCl aqueous solution, the RBIP pore diameter is 40 nm, the active area of the membrane is A = 0.32 cm².*

Comparison to electronic flashing ratchets

The RBIP described here is similar in function to flashing ratchets in the sense that particle transport is driven by internal potential fluctuations[2,3] and not by a voltage that is applied to external electrodes (as in rectifying ionic diodes[4,5] and rocking ratchets[2,3]). Thus, it is interesting to compare the obtained outputs to those reported in previous demonstrations of flashing ratchets. The ratio of the ratchet input signal amplitude, V_a, to the magnitude of the average output voltage, $\bar{V}_{out}$, or current, $\bar{I}_{out}$, are key parameters used to quantify the efficiency of a ratcheting process. In many of the previous demonstrations of flashing ratchets (which are closest in function to the RBIP reported here, but drove electrons or holes in semiconductors),[6–9] V_a is applied to electronic conductors that are insulated from the charge transport layer to avoid shunts. Since there is a significant electric potential drop across the insulation layers, a large input voltage amplitude is required. With the RBIP architecture, the input signal, V_a, is applied to the metal electrodes that are deposited on top of the AAO membrane and charge transport across the metal|solution interface is possible only by inducing redox reactions. Thus, charge transport across this interface is negligible, if no exogenous species are added and/or the amplitude of V_a is kept small. As a result, there is no need to insulate the contacts between the ratchet and the media in which the output charge transport takes place, and thus lower input signals can be used. In the case of the RBIP discussed in Figure 1, a TiO_2 ALD layer is deposited on top of the contacts to protect it from degradation and to assure that no redox reactions take place at the contacts. Nevertheless, as demonstrated with the other tested samples, this insulation layer is not strictly necessary, since the RBIP can drive ion transport with no associated redox reactions even without this layer (Figure 2-3, and the section "*Additional results and methods"* in the supporting information).

Calibration of V_{out} response from aqueous HCl concentration ratios across an RBIP

The correlation between the aqueous HCl concentration differences and the Ag/AgCl voltage was obtained by measuring the voltage between two Ag/AgCl wires placed in a cell filled with two solutions with predefined concentrations. An annealed AAO wafer with a pore diameter of 40 nm, and without deposited contacts, was used to separate the two cell compartments. Figure S17 shows the measured voltage as a function of the concentration ratio between the cells. However, it should be noted that variability between samples, the effect of the contacts, and changes in the pore surface charge due to the long exposure to acidic conditions, may lead to an inaccuracy in the concentration difference estimation.

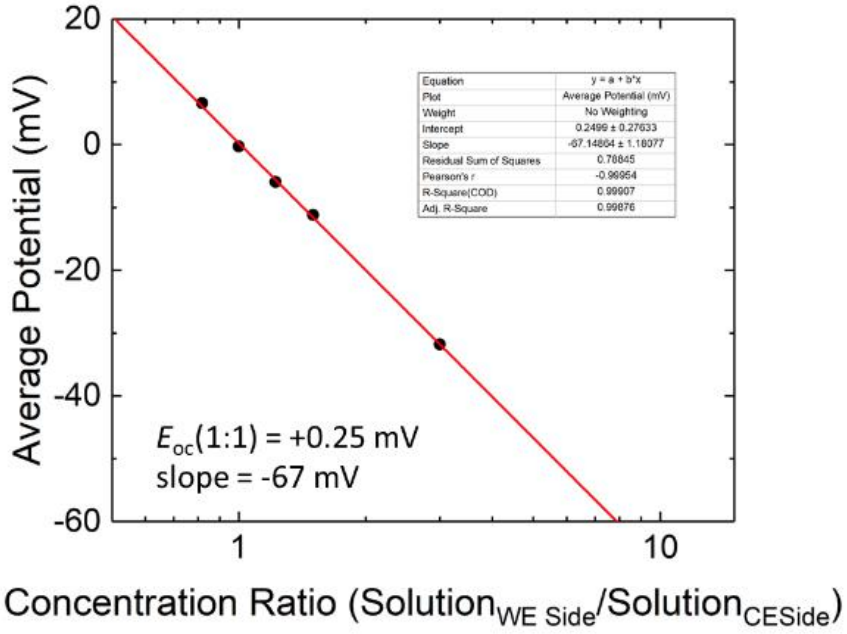

Figure S17: Measured voltage between two Ag/AgCl wires across an annealed AAO wafer with no contacts deposited, when a concentration gradient was intentionally introduced between the two compartments. The reference concentration is aqueous 1 mM HCl.

Sample degradation

As prepared samples have shown a pumping performance that is significantly higher than presented in Figure S9. However, this higher performance degraded in the first several hours of operation. Figure S18a shows the recorded output of the RBIP discussed in Figure S9 during its first 20 h of its operation. In this measurement, the as-prepared RBIP was operated continuously with an input signal as described in Figure S9a, with an amplitude of 0.4 V, until its performance stabilized. Only once the performance has stabilized the measurements presented in Figure S9a-d where conducted. In many of the tested samples post-mortem analysis revealed no noticeable changes in morphology. In such cases, failure may be a result of changes in the surface charge distribution within the pores leading to a change in the electric potential distribution within the RBIP. In other samples structural changes were visible. Figure S18b shows an EDS map overlaid on top of an SEM image of an as-prepared RBIP in which the contacts were deposited with electron beam evaporation. As shown in Figure S18b, the as-prepared samples have a uniform coverage of gold which allows effective biasing of the pores. Samples prepared with other methods had a similar structure. Figure S18c-d shows respectively an SEM image and an EDS map overlaid on top of the SEM

image of an RBIP that was operated for about 24 h. As can be seen in Figure S18c-d, clustering of gold forms islands that block some of the pores but also prevents effective biasing of the pores that are not blocked thus leading to a significant reduction in the pumping performance. In other samples, failure was a result of contact delamination from the AAO substrate.

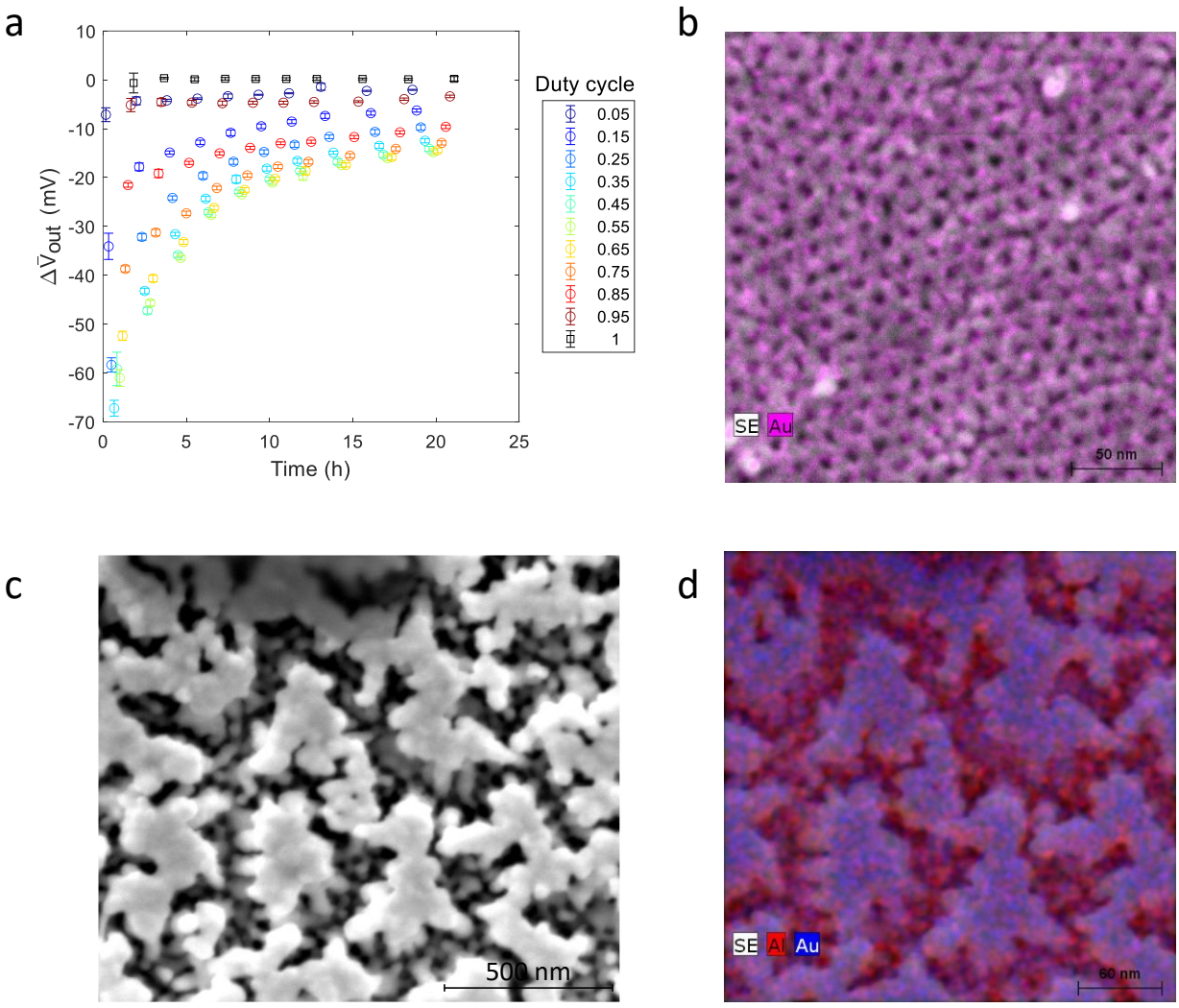

Figure S18: Stability analysis of an RBIP. (a) Ratchet output of an as-deposited sample cycled between different duty cycles for 21 h. (b) SEM and EDS overlay of an as-deposited sample with 20 nm pores. (c-d) SEM image and EDS of a sample after 25 h of operation.

Failure modes

The trivial failure modes that can affect the RBIP performance are the shunting and blocking of pores. Understanding the effect of these failure modes can help shed light on the contributions to the performance of different devices. When entire pores, or parts of the pores, are shunted, the electric potential distribution within the shunted regions is unaffected by the ratchet signal. As a result, the shunted regions provide a path for ions to diffuse back toward their equilibrium distribution, and thus limiting the RBIP pumping performance. When the salinity level is too high, such that the Debye length is

significantly smaller than the pore radius, the center of the pore will not be perturbed by the ratchet signal thus forming a shunt. Another cause for pore shunting is improper biasing of the pore, for example when the deposited metal layer does not cover the entire surface of the AAO wafer.

When pores are blocked, or when the resistance to transport through them is too high, the device can be effectively described as two separate compartments where the voltage difference between the two compartments is determined by the ratchet signal. In such case, the time averaged voltage output, $\Delta\bar{V}_{out}$ is simply the average voltage applied to the RBIP, and thus it is linear with the duty cycle. Furthermore, if the pores are almost entirely blocked, the output is less affected by changes in the solution conductivity. Figure S19a-b shows an example of the output of an RBIP with blocked pores. The RBIP pore diameter is 20 nm and the deposited metal layers are 40 nm of titanium (adhesion layer) and 40 nm of gold (planar equivalent). Figure S19a shows the measured V_{out} for an input signal with V_a of 0.2 V, a frequency of 100 Hz, and duty cycles between 5% and 95%. All the measurement parameters are as in Figure S9a. The aqueous solution is 1 mM KCl and 10 mM KCl. Figure S19b shows the extracted $\Delta\bar{V}_{out}$ as a function of the input signal duty cycle. The linear relation between the output and the duty cycle, and the small change of output with the salinity indicates that transport through the pores is too resistive or that the pores are blocked. Similarly, when an alumina membrane was used that did not intentionally have pores in it, $\Delta\bar{V}_{out}$ values were largest for 0% and 100% duty cycle, and zero for 50% duty cycle, further supporting a ratchet-based mechanism for our RBIPs.

Clearly, some devices may have regions that operate well, regions that are fully or partially shunted and other regions that are fully or partially blocked. In such case, the measured signal will be a convolution of the ratchet output, which is zero at duty cycles of 0% and 100% but is nonzero elsewhere; the contribution of shunted regions, which is zero for all duty cycles; and the contribution of highly resistive or blocked regions, which is linear with the duty cycle. Thus, partially blocked areas, or high resistance for ion transport within the pore, may be the reason for the non-zero $\Delta\bar{V}_{out}$ obtained in RBIPs with pore diameter of 20 nm. Figure S20 shows another example for $\Delta\bar{V}_{out}$ as a function of the duty cycle for an RBIP where the pores are partially blocked. The sample and input signal parameters are as in Figure 2 and the aqueous solution is 1mM HCl. The output curve is superimposed on a linear trend which is indicative of partial blockage of the pores.

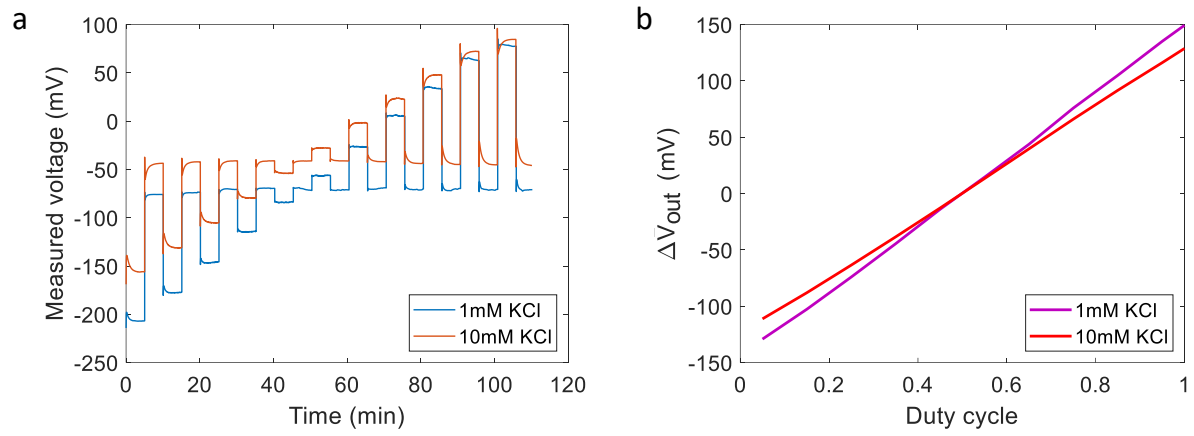

Figure S19: *Ratchet output for an RBIP with partially blocked 20 nm pores. (a) Measured output voltage for an input signal with various duty cycles. The input signal is a square wave with V_a of 0.2 V and the frequency is 100 Hz. (b) Time averaged output voltage, $\Delta\bar{V}_{out}$, as a function of the input signal duty cycle.*

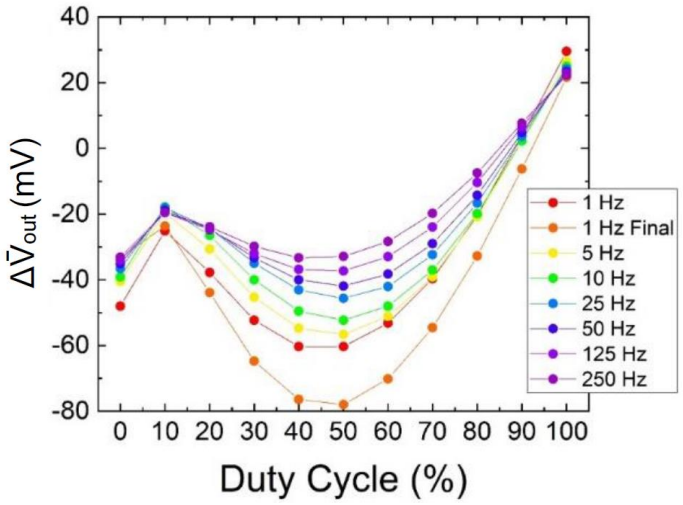

Figure S20: Output voltage as a fucntion of the duty cycle for an RBIP with partially blocked pores. The sample and input signal parameters are as in Figure 2 and the electrolyte is 1 mM HCl aqueous solution.

RBIP simulation

To estimate the ratchet-induced voltage between the two Ag/AgCl wires we assume that the voltages between the RBIP contacts and the Ag/AgCl wires next to them (V_L and V_R) can be modeled as charging and discharging capacitors. Figure S21a shows an illustration of the system and an equivalent circuit describing its operation.

The resting potential difference between each of the ratchet contacts and the wire next to it are $V_{R,eq}$ and $V_{L,eq}$, where subscript L,R denote left and right in Figure 1a and Figure S21a. In equilibrium $V_L = V_{L,eq}$ and $V_R = V_{R,eq}$. Since the ratchet is floating with respect to the wires, when a bias V_a is applied, one metal contact is charged, and the other is discharged. However, the bias is not necessarily shared equally between the two contacts. We assign the parameter a to describe this source of asymmetry (yet, in all the subsequent results we assume that the charging is symmetric, i.e., a = 0.5*)*. If the input signal has a very

long temporal period compared to the time constants for charging and discharging, the voltages in the system will reach their steady state values. For the first part of the period, the steady state voltages V_{Lf} and V_{Rf} are:

$$V_L = V_{Lf,1} = V_{L,eq} - aV_a; \quad V_R = V_{Rf,1} = V_{R,eq} + (1-a)V_a. \tag{S1}$$

We use subscript 1 to denote the first part of the temporal period ($t < d_cT$) where d_c is the duty cycle and T is the signal period. The second part of the period ($t > d_cT$), is noted with subscript 2. In this case the steady state voltages follow:

$$V_L = V_{Lf,2} = V_{L,eq} + (1-a)V_a; \quad V_R = V_{Rf,2} = V_{R,eq} - aV_a. \tag{S2}$$

According to the definitions in Figure 1a, the output voltage, V_{out} follows:

$$V_{out} = V_L + V_{in} - V_R. \tag{S3}$$

In steady state conditions for a positive voltage applied on the ratchet:

$$V_{out} = V_{L,eq} - aV_a + V_a - V_{R,eq} - (1-a)V_a = V_{L,eq} - V_{R,eq} = \Delta V_{eq}. \tag{S4}$$

Thus, in steady state conditions, the application of a constant bias does not drive the device away from its equilibrium voltage. Furthermore, in a perfectly symmetric system, the equilibrium voltages for the two surfaces are the same, and the steady state output voltage will be 0.

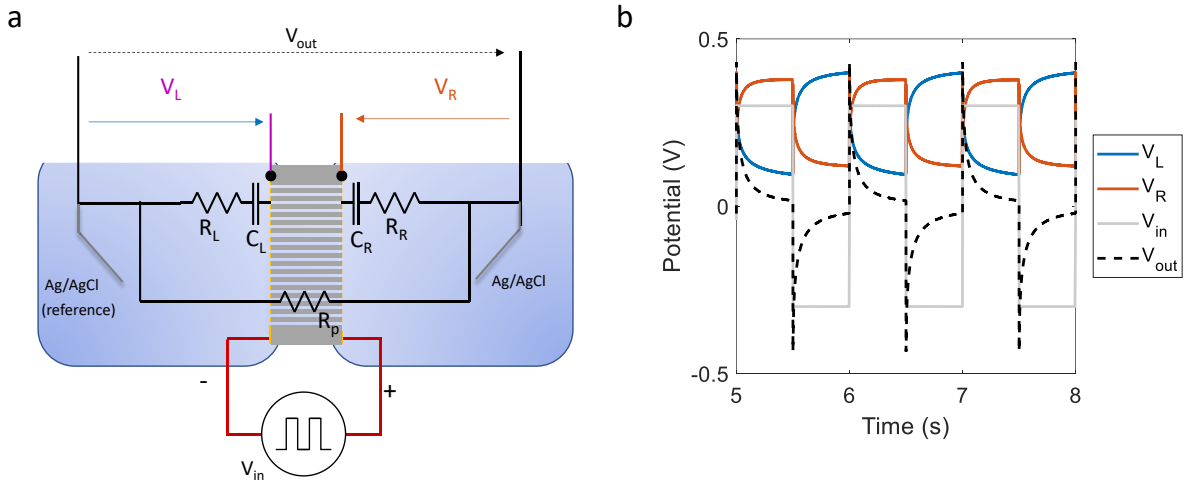

Figure S21: (a) Illustration of the ratchet setup with all the measured signals and an equivalent circuit. (b) Measured voltages during ratchet operation. The frequency is 1 Hz, the duty cycle is 0.5 and the amplitude is V_a =0.3 V. The RBIP was prepared as the one described in Fig 2 and the electrolyte is 1 mM KCl aqueous solution.

Figure S21b shows an example of signals measured in response to an input signal with a 0.5 duty cycle, a frequency of 1 Hz, and an amplitude of V_a = 0.3 V. The RBIP was prepared as the one discussed in Fig 2, and the electrolyte is 1 mM KCl aqueous solution. The voltage signals V_L and V_R can be approximately described by a single exponent charging function defined by their initial voltage V_i, its time constant, τ, and the steady state voltage, V_f:

$$V(V_i, V_f, \tau, t) = V_f + (V_i - V_f)\exp\left(-\frac{t}{\tau}\right). \tag{S5}$$

In non-linear systems such as electric double layers, the time constant depends on potential, frequency, and duty cycle. The acceptable exponential fit to our experimental data (Figure 1, Figure S2, Figure S4-

Figure S6, Figure S8) suggests that that for our RBIPs, this non-linearity can be described through the different time constants for charging and discharging the contacts. Thus, for a given frequency and duty cycle the transients will be determined by two time constants, $\tau_1(d_c, f)$ and $\tau_2(d_c, f)$.

In the first part of every period, the input voltage is V_a. Thus, V_L discharges towards $V_{Lf,1}$ with a time constant of $\tau_{L,1}$:

$$\begin{aligned} V_{L,1}(t) &= V_{Lf,1} + \left(V_{Li,1} - V_{Lf,1}\right)\exp\left(-\frac{t}{\tau_{L,1}}\right) \\ &= V_{L,eq} - aV_a + \left(V_{Li,1} - V_{L,eq} + aV_a\right)\exp\left(-\frac{t}{\tau_{L,1}}\right). \end{aligned} \tag{S6}$$

$\mathrm{V_R}$ charges towards $V_{Rf,1}$:

$$\begin{aligned} V_{R,1}(t) &= V_{Rf,1} + \left(V_{Ri,1} - V_{Rf,1}\right)\exp\left(-\frac{t}{\tau_{R,1}}\right) \\ &= V_{R,eq} + (1-a)V_a \\ &\quad + \left(V_{Ri,1} - V_{R,eq} - (1-a)V_a\right)\exp\left(-\frac{t}{\tau_{R,1}}\right). \end{aligned} \tag{S7}$$

$V_{Li,1}$ and $V_{Ri,1}$ are calculated assuming that the V_R and V_L are continuous, and that the system is operating periodically in steady state.

For the second part of every period, we get:

$$\begin{aligned} V_{L,2}(t) &= V_{Lf,2} + \left(V_{Li,2} - V_{Lf,2}\right)\exp\left(-\frac{t - d_cT}{\tau_{L,2}}\right) \\ &= V_{L,eq} + (1-a)V_a \\ &\quad + \left(V_{Li,2} - V_{leq} - (1-a)V_a\right)\exp\left(-\frac{t - d_cT}{\tau_{L,2}}\right), \end{aligned} \tag{S8}$$

and:

$$\begin{aligned} V_{R,2}(t) &= V_{Rf,2} + \left(V_{Ri,2} - V_{rf,2}\right)\exp\left(-\frac{t - d_cT}{\tau_{R,2}}\right) \\ &= V_{R,eq} - aV_a + \left(V_{Ri,1} - V_{Req} + aV_a\right)\exp\left(-\frac{t - d_cT}{\tau_{R,2}}\right). \end{aligned} \tag{S9}$$

Periodicity implies that:

$$\begin{aligned} V_{L,1}(t = 0) &= V_{L,2}(t = T), \\ V_{L,1}(\,t = d_cT) &= V_{L,2}(t = d_cT). \end{aligned} \tag{S10}$$

Inserting and noting $A_L = \exp\left(-\frac{d_cT}{\tau_{L,1}}\right)$, $\mathrm{B}_L = \exp\left(-\frac{(1-d_c)T}{\tau_{L,2}}\right)$:

$$\begin{aligned} V_{Li,1} &= V_{Lf,2} + \left(V_{Li,2} - V_{Lf,2}\right)\exp\left(-\frac{T(1-d_c)}{\tau_{L,2}}\right) = V_{Lf,2} + \left(V_{Li,2} - V_{Lf,2}\right)\mathrm{B}_L, \\ V_{Li,2} &= V_{Lf,1} + \left(V_{Li,1} - V_{Lf,1}\right)\exp\left(-\frac{Td_c}{\tau_{L,1}}\right) = V_{Lf,1} + \left(V_{Li,1} - V_{Lf,1}\right)A_L. \end{aligned} \tag{S11}$$

Inserting one into the other and extracting $V_{Li,2}$:

$$V_{Li,2} = \frac{V_{Lf,1} + (V_{Lf,2} - V_{Lf,1})A_L - \mathrm{B}_L A_L V_{Lf,2}}{1 - \mathrm{B}_L A_L}. \tag{S12}$$

Similarly for V_R:

$$\begin{aligned} V_{R,1}(t = 0) &= V_{R,2}(t = T\,), \\ V_{R,1}(\,t = d_c T) &= V_{R,2}(t = d_c T). \end{aligned} \tag{S13}$$

Noting $A_R = \exp\left(-\frac{d_c T}{\tau_{r,1}}\right)$, $B_R = \exp\left(-\frac{(1-d_c)T}{\tau_{r,2}}\right)$, we obtain:

$$V_{Ri,2} = \frac{V_{Rf,1} + \left(V_{Rf,2} - V_{Rf,1}\right)A_R - B_R A_R V_{Rf,2}}{1 - B_R A_R}. \tag{S14}$$

We can now find the output voltage at each stage:

$$V_{out} = V_L + V_{in} - V_R. \tag{S15}$$

Inserting:

$$\begin{aligned} V_{out,1} = V_{L,eq} - aV_a + \left(V_{Li,1} - V_{L,eq} + aV_a\right)\exp\left(-\frac{t}{\tau_{L,1}}\right) + V_a \\ - \Bigg[V_{Req} + (1-a)V_a \\ + \left(V_{Ri,1} - V_{R,eq} - (1-a)V_a\right)\exp\left(-\frac{t}{\tau_{R,1}}\right)\Bigg]. \end{aligned} \tag{S16}$$

Rearranging:

$$\begin{aligned} V_{out,1} &= \left(V_{L,eq} - V_{R,eq}\right) + \left(V_{Li,1} - V_{Leq} + aV_a\right)\exp\left(-\frac{t}{\tau_{L,1}}\right) \\ &\quad - \left(V_{Ri,1} - V_{Req} - (1-a)V_a\right)\exp\left(-\frac{t}{\tau_{R,1}}\right) \\ &= \Delta V_{eq} + \left(V_{Li,1} - V_{Lf,1}\right)\exp\left(-\frac{t}{\tau_{L,1}}\right) \\ &\quad - \left(V_{Ri,1} - V_{Rf,1}\right)\exp\left(-\frac{t}{\tau_{R,1}}\right). \end{aligned} \tag{S17}$$

And for the second part of the period:

$$\begin{aligned} V_{out,2} = V_{L,eq} + (1-a)V_a + \left(V_{Li,1} - V_{Leq} - (1-a)V_a\right)\exp\left(-\frac{t - d_c T}{\tau_{L,2}}\right) - V_a \\ - \left[V_{R,eq} - aV_a + \left(V_{Ri,1} - V_{R,eq} + aV_a\right)\exp\left(-\frac{t - d_c T}{\tau_{R,2}}\right)\right]. \end{aligned} \tag{S18}$$

Rearranging:

$$
\begin{aligned}
V_{out,2} &= V_{L,eq} - V_{R,eq} + \left(V_{Li,1} - V_{L,eq} - (1-a)V_a\right)\exp\left(-\frac{t-d_cT}{\tau_{L,2}}\right) \\
&\quad - \left[\left(V_{R,i,1} - V_{R,eq} + aV_a\right)\exp\left(-\frac{t-d_cT}{\tau_{R,2}}\right)\right] \\
&= \Delta V_{eq} + \left(V_{Li,2} - V_{Lf,2}\right)\exp\left(-\frac{t-d_cT}{\tau_{L,2}}\right) \\
&\quad - \left(V_{Ri,2} - V_{Rf,2}\right)\exp\left(-\frac{t-d_cT}{\tau_{R,2}}\right).
\end{aligned}
\tag{S19}
$$

From equations (S17) and (S19) we can see that the net voltage is a result of the difference between the charging and the discharging of the two surfaces over the course of one period.

The time averaged voltage is found by integrating V_{out}:

$$
\begin{aligned}
\bar{V}_{out} &= \frac{1}{T}\left[\int_0^{d_cT} V_{out,1}dt + \int_{d_cT}^{T} V_{out,2}dt\right] = \\
&= \Delta V_{eq} \\
&\quad + \frac{1}{T}\left\{\tau_{L,1}\left(V_{Li,1} - V_{Lf,1}\right)\left[1 - \exp\left(-\frac{d_cT}{\tau_{L,1}}\right)\right]\right. \\
&\quad - \tau_{R,1}\left(V_{Ri,1} - V_{Rf,1}\right)\left[1 - \exp\left(-\frac{d_cT}{\tau_{R,1}}\right)\right] \\
&\quad + \tau_{L,2}\left(V_{Li,2} - V_{Lf,2}\right)\left[1 - \exp\left(-\frac{(1-d_c)T}{\tau_{L,2}}\right)\right] \\
&\quad \left. - \tau_{R,2}\left(V_{Ri,2} - V_{Rf,2}\right)\left[1 - \exp\left(-\frac{(1-d_c)T}{\tau_{R,2}}\right)\right]\right\}.
\end{aligned}
\tag{S20}
$$

It can be easily shown that in a linear system where $\tau_{L,1} = \tau_{L,2}$ and $\tau_{R,1} = \tau_{R,2}$ the $\bar{V}_{out}$ is 0. However, if the capacitances are nonlinear such that the time constants are different, non-zero values for $\bar{V}_{out}$ can be obtained. If the time constants are only determined by the duration of the two portions of the input signal (as demonstrated experimentally), then $\tau_{L,2} = \tau_{R,2}$ and $\tau_{L,1} = \tau_{R,1}$. In all the results presented here we have assumed that ΔV_{eq} is 0 V, and a is 0.5. Figure S22 shows the calculated ratchet output as a function of the duty cycle for several input signal frequencies using the time constants shown in Figure 1h for a duty cycle of 0.5: $\tau_{L,1} = 6.59$ ms, $\tau_{R,1} = 7.23$ ms, $\tau_{L,2} = 8.5$ ms, and $\tau_{R,2} = 8.21$ ms. Even for such a small difference in time constants a significant output is obtained. However, since the model does not account for changes in the saturation voltage V_f, and the effective amplitude V_i-V_f with the duty cycle, it cannot fully reproduce the measured outputs.

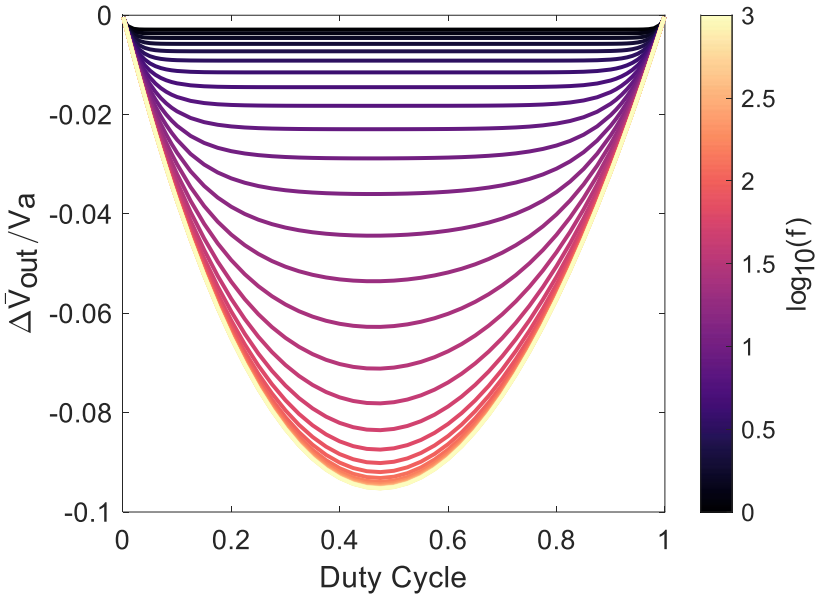

Figure S22: The ratchet normalized output, $\Delta\bar{V}_{out}/V_a$, as a function of the input signal duty cycle for several input signal frequencies. The time constants are taken from Figure 1h for a duty cycle of 0.5: $\tau_{L,2} = 8.5$ ms, $\tau_{R,2} = 8.21$ ms, $\tau_{L,1}$ =6.59 ms, $\tau_{R,1} = 7.23$ ms.

It is interesting to show the requirements for obtaining a non-zero output for a time-symmetric input signal (d_c = 0.5). Inserting $d_c = 0.5$, $\tau_{L,1} = \tau_{R,1}$, $\tau_{L,2} = \tau_{R,2}$, and $\Delta V_{eq} = 0V$ into equation (S20) we obtain:

$$\frac{\Delta\bar{V}_{out}}{V_a} = \frac{2}{T}\frac{\left(1-\mathrm{e}^{-\frac{T}{2\tau_{L,1}}}\right)\left(1-\mathrm{e}^{-\frac{T}{2\tau_{R,2}}}\right)}{1-\mathrm{e}^{-\frac{T}{2}\left(\frac{1}{\tau_{L,1}}+\frac{1}{\tau_{R,2}}\right)}}\left(\tau_{L,1}-\tau_{R,2}\right) \qquad \text{(S21)}$$

Thus, any difference between the charging (and discharging) time constants of the two surfaces results in a non-zero output and the longer time constant determines the direction of the driving force. Figure S23 shows the calculated normalized output $\Delta\bar{V}_{out}/V_a$ as a function of $\tau_{L,1} = \tau_{R,1} = \tau$ with $\tau_{L,2} = \tau_{R,2} = \tau_{ref} = 8.5\,ms$ and $d_c = 0.5$.

In a symmetric device both surfaces charge (and discharge) with the same time constants: $\tau_{R,1} = \tau_{L,2}$ and $\tau_{R,2} = \tau_{L,1}$. Under such conditions the output is zero for a $d_c = 0.5$, but can be non-zero for other duty cycle values. Figure S24 shows the ratchet normalized output as a function of the input signal duty cycle for several input signal frequencies. The charging time constants for both surfaces are $\tau_{R,1} = \tau_{L,2} = 8\,ms$, and the discharging time constants are $\tau_{R,2} = \tau_{L,1} = 6\,ms$. Similar to an anti-symmetric flashing ratchet,[10] the ratchet output is zero at duty cycles of 0,0.5 and 1 and is anti-symmetric about $d_c = 0.5$. Thus, in a symmetric system, a non-zero output can be obtained when the capacitances are nonlinear, and the input signal is not time symmetric ($d_c \neq 0.5$).

The suggested model shows that a non-linear capacitance is essential for an RBIP to operate. However, to fully predict and model the performance of real devices, the non-linear correlation between the input

signal parameters and the charging and discharging time constants must be found. Since the frequency dispersion of the double layer capacitance is heavily affected by surface roughness, material crystallinity, and other micro-scale properties,[10,11] such analyses must be conducted for every RBIP material and fabrication process separately and is left for future work. The model assumes that the resistance for ion transport through the pores, R_p is very high thus it accounts only for open-circuit conditions as in Figure 1i and Figure 2a-c. An equivalent circuit model that accounts for ion transport through the pores and the Ag/AgCl wires electrochemical reactions can be used to analyze other operating points. Nevertheless, as demonstrated in Figure 2g, when the Ag/AgCl auxiliary electrodes assure that charge neutrality is maintained, the RBIP operation can be modeled as a voltage source in parallel to a resistive element which accounts for charge transport through the pores. A more thorough analysis of equivalent circuit models for the RBIP is left for future work.

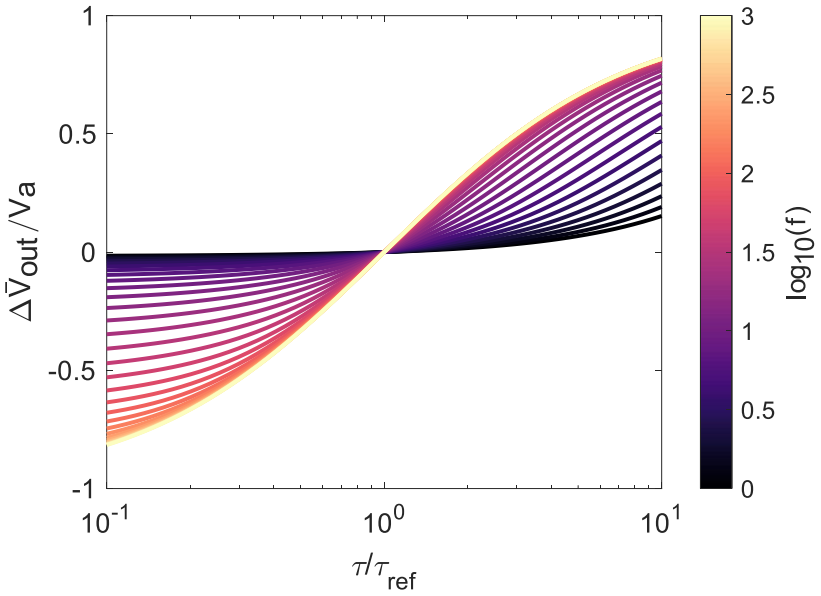

Figure S23: the calculated normalized output $\Delta\bar{V}_{out}/V_a$ as a function of $\tau_{L,1} = \tau_{R,1} = \tau$ with $\tau_{L,2} = \tau_{R,2} = \tau_{ref} = 8.5\ ms$ and $d_c = 0.5$.

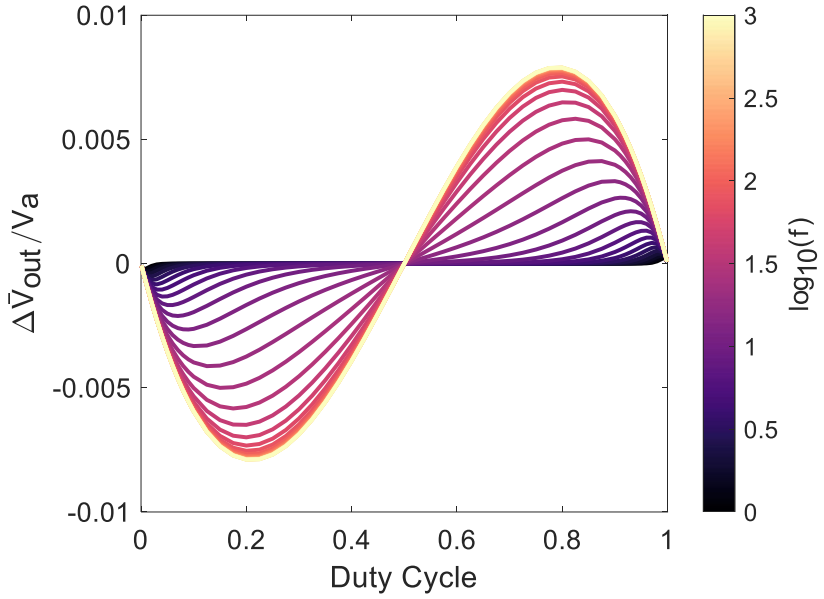

Figure S24: the ratchet normalized output as a function of the input signal duty cycle for several input signal frequencies. The charging time constants for both surfaces are $\tau_{R,1} = \tau_{L,2} = 8\ ms$*, and the discharging time constants are* $\tau_{R,2} = \tau_{L,1} = 6\ ms$*.*

An RBIP driven dialysis system

Figure S25 shows a schematic illustration of an RBIP driven dialysis system. The system is comprised of two compartments separated by two RBIPs placed in parallel and operated with two independent input signals. The RBIPs and input signals are such that one RBIP drives cations to the concentrate compartment and the other pumps anions to the concentrate compartment. To avoid ion backflow, the RBIP driving cations to the concentrate compartment is coupled to a cation exchange membrane (CEM) and the other to an anion exchange membrane (AEM). Since both devices pump ions from the same source compartment towards a shared concentrate compartment desalination is achieved.

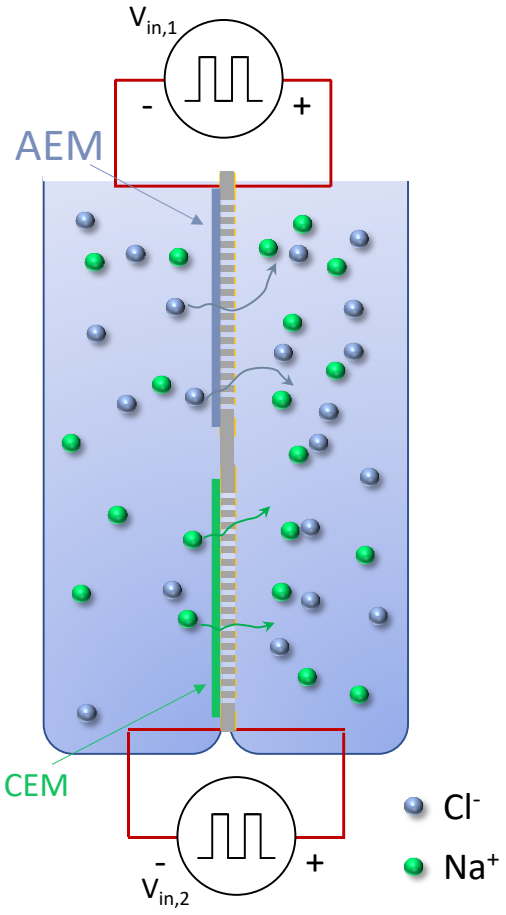

Figure S25: a schematic illustration of an RBIP driven dialysis system.

References

1. Bazant, M. Z., Kilic, M. S., Storey, B. D. & Ajdari, A. Towards an understanding of induced-charge electrokinetics at large applied voltages in concentrated solutions. *Adv. Colloid Interface Sci.* **152**, 48–88 (2009).

2. Hänggi, P. & Marchesoni, F. Artificial Brownian motors: Controlling transport on the nanoscale. *Rev. Mod. Phys.* **81**, 387–442 (2009).

3. Reimann, P. Brownian motors: Noisy transport far from equilibrium. *Phys. Rep.* **361**, 57–265 (2002).

4. Siwy, Z. & Fuliński, A. A nanodevice for rectification and pumping ions. *Am. J. Phys.* **72**, 567–574 (2004).

5. Siwy, Z. & Fuliński, A. Fabrication of a Synthetic Nanopore Ion Pump. *Phys. Rev. Lett.* **89**, 4–7 (2002).

6. Kedem, O., Lau, B. & Weiss, E. A. How to Drive a Flashing Electron Ratchet to Maximize Current. *Nano Lett.* **17**, 5848–5854 (2017).

7. Kedem, O., Lau, B., Ratner, M. A. & Weiss, E. A. Light-responsive organic flashing electron ratchet. *Proc. Natl. Acad. Sci.* **114**, 8698–8703 (2017).

8. Kedem, O., Lau, B. & Weiss, E. A. How to Drive a Flashing Electron Ratchet to Maximize Current. *Nano Lett.* **17**, 5848–5854 (2017).

9. Roeling, E. M., Germs, W. C., Smalbrugge, B., Geluk, E. J., de Vries, T., Janssen, R. A. J., & Kemerink, M. Organic electronic ratchets doing work. *Nat. Mater.* **10**, 51–55 (2011).

10. Rozenbaum, V. M., Shapochkina, I. V., Teranishi, Y. & Trakhtenberg, L. I. Symmetry of deterministic ratchets. *Phys. Rev. E* **100**, 22115 (2019).